Cape Peninsula
University of Technology

Design and Manufacturing of a Temperature Controlled Chamber for a Tensile Testing Machine

by

Zamavangeli Mdletshe

Thesis submitted in fulfilment of the requirements for the degree

Master of Engineering: Mechanical Engineering

in the Faculty of Engineering

at the Cape Peninsula University of Technology

Supervisor: Dr V. Msomi

Bellville

November 2017

DECLARATION

I, Zamavangeli Mdletshe, declare that the contents of this thesis represent my own unaided work, and that the thesis has not previously been submitted for academic examination towards any qualification. Furthermore, it represents my own opinions and not necessarily those of the Cape Peninsula University of Technology.

Signed **Date**

ABSTRACT

Material testing is an important test to researchers in material science fields and other engineering related fields. This is the base for material evaluation prior to the application. This test is used in the engineering field to determine the strength of materials which is an aspect of assigning materials to different functions. The uniaxial tensile testing of material is the most common form of testing the strength of metallic material - usually to investigate whether or not the material is worthy of the intended application.

Material testing is normally performed under uncontrolled conditions in most laboratories. Numerous attempts had been previously made in attempt to control the temperature conditions when performing the tensile test on special materials such as shape memory alloys (SMA) and other smart materials. Various methods had been employed to control the temperature during tensile testing, methods such as induction heating, warm liquid baths, etc.

The aim of this study was to develop a temperature controlled environment for the *Houndsfield* tensile testing machine which is found at the Cape Peninsula University of Technology in the Mechanical Engineering Department workshop. This was achieved through designing and manufacturing of a thermally controlled chamber -better known as a furnace. This chamber was tested for the optimal combination of proportional, integral and derivative parameters which were tuned on the proportional integral derivative (PID) controller.

Performing the tensile test under controlled thermal conditions will allow the analysis of SMAs and other materials behaviour at different temperatures. With the aid of the manufactured chamber, the superior features of the SMA will be able to be studied. The manufactured thermal chamber which is electrically powered is insulated with a special ceramic refractory material to prevent the heat from escaping the chamber. The PID controller was used to control the temperature and heating elements act as the heat source.

The manufactured chamber could withstand the maximum temperature 350^{o}C that it was initially designed for. However, the challenge of having the specimen to be tested fully inside the chamber was overcame by designing specimen connectors that connected the specimen to the tensile testing machine. Tensile tests were conducted on the SMA wire at room temperature and other various controlled temperatures and different behaviours were observed on the stress-strain graphs.

ACKNOWLEDGEMENTS

Firstly, I would like to thank the Almighty for seeing me through till this stage.

Secondly, I thank my supervisor Dr V. Msomi for his guidance and patience and most of all for believing in me to carry out this research. Thank you Baba Nomndayi.

I would also like to thank Dr O. Nemraoui for his selfless help throughout the manufacturing process of the project. Thank you.

I thank the Mechanical Engineering Department technical staff for their help, I highly appreciate.

The financial assistance of the National Research Foundation towards this research is acknowledged.

I would also like to thank my parents for allowing me to study further to this level. I also thank my siblings Njabulo, Sphakahle and Gugulabadletshe thank you for all the love, support and motivation that you'll gave me. Special thanks to my grandmother and my late grandfather who passed away during the compilation of this thesis. Thank you boNgomane.

Last but not least I thank my partner in all Lungisile Kweyama for helping me in every possible way and for being there for me throughout my studies. May his grace, shine upon you.

Table of Contents

LIST OF FIGURES

LIST OF TABLES

GLOSSARY

Terms/Acronyms/Abbreviations	Definition/Explanation
CPUT	Cape Peninsula University of Technology
^{O}C	Degrees Celsius
SSR	Solid State Relay
PID	Proportional Integral Derivative
SV	Set/Desired Value
PV	Process/Actual Value
T_x	Temperature at x
A	Surface/cross-sectional area
os	overshoot
SMA	Shape memory alloy
SME	Shape memory effect
SE	Superelasticity/pseudoelesticity
Range band	Variation of values according to the scale

CHAPTER 1
INTRODUCTION

1.1 PROBLEM STATEMENT

The tensile test is a useful test that contributes greatly to material testing (Kutz, 2013) . Tensile tested materials enable proper assignment of materials to suitable engineering applications. According to Loveday et al. (2004) the strength of a material under tension has long been regarded as one of the most important characteristics required for design, production quality control and life production of industrial plants. Uniaxial tensile testing of a material is the most common type of material test used to determine the strength of metallic materials; it is usually used to investigate the worthiness or suitability of a material for an intended application (Han, 1992).

Different materials exhibit different mechanical properties under physical or thermal loading. Most metallic materials are tested for their mechanical properties at room temperature. However, some materials such as shape memory alloy (SMA) and other smart materials in general require controlled or elevated temperature conditions in order for them to exhibit their mechanical properties. SMA materials in particular have mechanical properties that mainly depend on temperature (Srinivasan and McFarland, 2001).

This makes it essential to isolate the testing conditions from the environmental conditions due to the fact that, isolated conditions mean that the test is performed under controlled conditions which yields to the better results. The practical method that could be used for isolating the two mentioned conditions from each other is to have a thermal controlled chamber surrounding the material being tested.

In this study a thermal chamber was designed, manufactured and tested in attempt to improve the testing conditions for the tensile testing machine in our workshop (Mech. Eng. - CPUT). Rather than having a thermal chamber separate from the tensile machine, this chamber is designed in a way that it can be attached (and detached) onto the tensile machine which allows the control of the temperature during the performance of tensile testing. This eliminates the time spent in transporting the specimen from a furnace to mounting or gripping it onto the tensile testing machine. Tensile testing materials at elevated temperature has become very popular with the discovery of shape memory alloy materials (Srinivasan and McFarland, 2001) which then gave rise to conducting this study. Therefore, the thermal chamber was conceptualized, designed, manufactured and thereafter tested. This thermal chamber is designed to suit our current *Houdsfield* tensile testing machine.

1.2 BACKGROUND

When the studies on the behaviour of shape memory alloy (SMA) at CPUT were conducted, it was not possible to achieve the tensile test data of the SMA specimen under controlled temperature instead all experiments were performed at room temperature (Msomi and Oliver, 2016) . This led to the achievement of a normal stress and strain graph similar to the one on Figure 1.1 which does not illustrate the two prominent properties of SMA, namely the shape memory effect (SME) and the super-elasticity (SE).

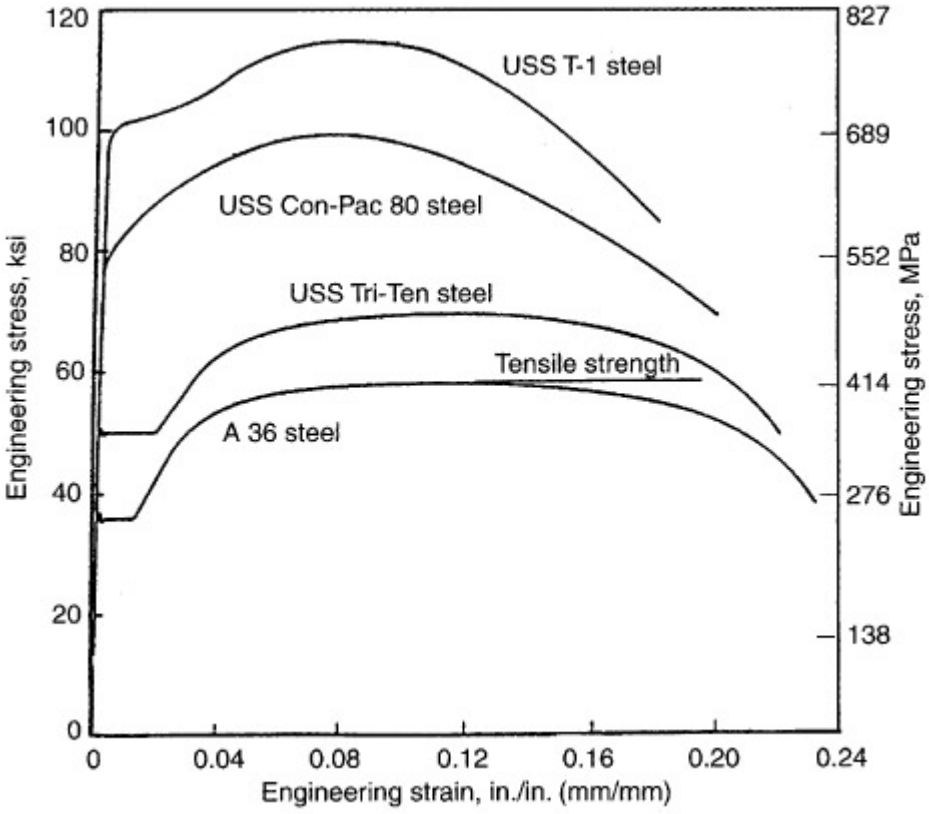

Figure 1.1: Typical stress-strain curve for structural steels having specific minimum tensile properties (Davis, 2004)

Shape memory effect (SME) is the ability of SMA to regain its original shape upon thermal application. Superelasticistity (SE) is the ability of SMA to fully recover and regain its shape when the mechanical

load is removed at temperature above austenite finish temperature. These two properties are clearly seen on Figure 1.2, justifying the need of the proposed thermal chamber.

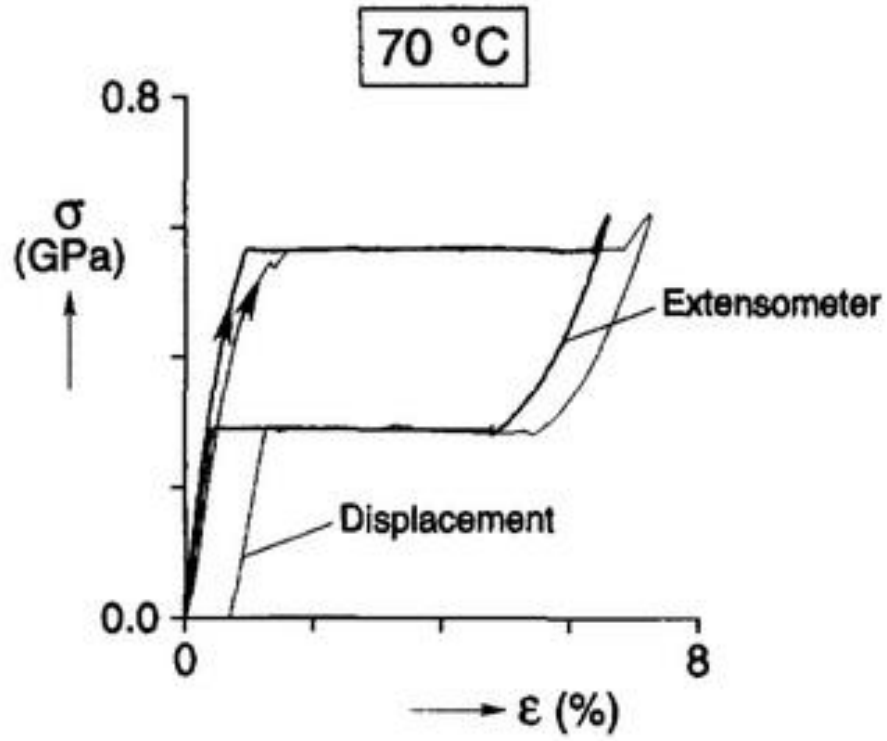

Figure 1.2: Stress and strain graph

(Shaw and Kyriakides, 1995)

The lack of isolated or controlled temperature conditions when using the tensile machine that is available in our workshop has led to this study in attempt to improve its versatility. Significant work was conducted by (Shaw and Kyriakides, 1995) where they were analysing the strength of material at controlled temperature using liquid bath to heat the surroundings of the specimen tested.

Shape training is a process of exposing SMA material to the fixed temperature of about 500^{o}C for it to have a specific permanent shape. An SMA (if it is wire) is clamped in any desired shape then heated, to effect the rearrangement of microstructure. The wire is quenched in liquid to register the new permanent shape. Should there be deformation to SMA wire which disturbs the trained shape, the lost shape could be regained upon thermal load application (Case et al., 2004).

Unlike other normal metallic materials, the stress and strain graph of a trained SMA illustrated on Figure 1.2 shows a closed loop graph that can be obtained with the success of the thermal chamber manufactured in this study.

1.3 OBJECTIVES

The primary objective of this study was to design and manufacture a temperature controlled chamber. In achieving the primary objective there were constraints and guidelines that were set and followed. Therefore, the objectives of the study were as follows:

a) The chambers maximum set point temperature was to be 350^{o}C.
   The design calculations of the heating elements were done to ensure that the selected heating elements can handle the maximum operating temperature within the heat chamber.

b) The chamber was to not interfere with the normal functioning of the tensile machine.
   When the chamber is detached, the tensile machine should be able to continue its fundamental function without trouble induced by the chamber.

c) The chamber had to be detachable and attachable onto the *Houndsfield* machine.
   The chamber must be removable from the tensile machine after performing a controlled tensile test. The chamber is specifically designed for the *Houndsfield* Mechanical Engineering Department's tensile testing machine. All design dimensions for the chamber are made with reference to this machine.

d) Designing of chamber
   Using *solidworks,* the designs were produced in 2D manufacturing detailed drawings and assembly draw in 2D and 3D.

e) Heating source had not to be in contact with the specimen tested.
   The temperature probe detecting the actual temperature within the heat chamber should be close enough to the specimen being tested but not in direct contact with it.

f) The chamber's control system must be able to hold the temperature for 10 to 25 minutes at steady state.
   The system had to reach steady state at the shortest possible time and these conditions were to be held at least a minimum of 10 to 25 minutes.

g) Experimental tuning
   The tuning of the controller was to be done experimentally. The behaviour of the temperature against time was recorded with the aid of a *Explore GLX* data logger. PID parameters that yielded the system to reach the desired temperature in the shortest time were investigated experimentally.

h) Testing of the chamber
   After the ideal combination of parameters had been found, testing of the maximum temperature was done to check the body temperature of the chamber with the aid of the infrared thermometer.

1.4 DESIGN OVERVIEW

The proposed chamber was designed to be attached on to the existing tensile machine at the Mechanical Engineering Department at CPUT. Therefore, the chamber was to fit in the working space illustrated in figure 1.3. However, the grips were not to be inside the chamber. Hence the connectors were initially introduced according to Figure 1.3.

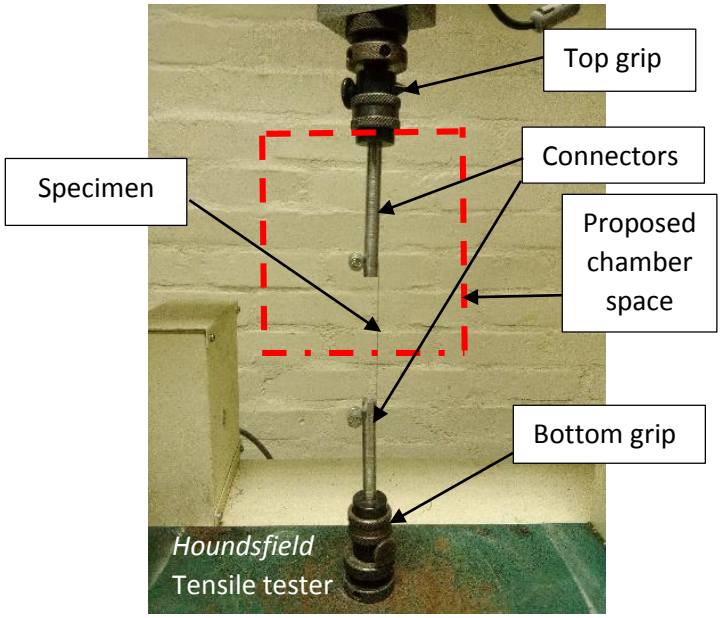

Figure 1.3: Working space

There are various kinds of methods of controlling test conditions from the environment, which are all based on the three fundamental thermodynamics theories of heat transfer namely the convection, conduction and radiation. The approach that was taken in this work to control the temperature conditions was by means of thermal chamber or furnace in simple terms. Convection heating was used to generate the temperature within this chamber. The refractory lining of the chamber was manufactured using the *JM23 energy saving fire bricks* as the insulator. Two *Kanthal D* heating elements connected in series were used to radiate the heat sideways in the system, which were electrically powered.

Controlling of the temperature was achieved by the use of a proportional integral derivative (PID) process control unit *EMKO ESMM-XX30*. This device with the help of the solid state relay (SSR) enables the end user to set any desired temperature ranging from room temperature to maximum operating temperature (350^{o}C) of the designed and manufactured chamber. The k-type thermo-couple (which served as the sensor) probed the actual temperature readings, which continuously sends feedback to the PID controller for it to configure the actual temperature to the one desired by the user. Therefore,

on the controller display one would perceive the desired or set temperature value (at the bottom in green colour on the controller display) and the system or actual process temperature value (at the top in red colour on the controller display), after a certain period the top reading has to stabilize to the set value or desired temperature.

It should to be noted that this work was experimental research. Therefore, modelling or simulation of the PID tuning was not part of the objectives. Hence, the ideal combination of parameters of the PID controller were obtained experimentally. The testing and evaluation stage of the chamber was mostly testing for the shortest time taken for the desired temperature to be reached and the efficiency of the parameters at the maximum temperature. Finally, the overall function of the chamber was tested and this depended on the programming of the PID controller.

1.5 THESIS OVERVIEW

Chapter 1 – Introduction

In this chapter the problem statement, background, objectives are listed and the overview of this study is presented subsequently.

Chapter 2 – Literature Review

This chapter addresses the literature on furnaces. It goes on to review literature that distinguishes the difference between laboratory and industrial furnaces. The different types of tensile tests are reviewed. Then the elevated temperature testing of materials including shape memory alloys are reviewed.

Chapter 3 – Design and Manufacturing of Chamber

In this chapter the design of the chamber is presented. Detailed drawing and all steps and stages undergone are clearly shown. Calculations that were done for the refractory and heating element selection are presented.

Chapter 4 – Experimental Performances

The experimental setups and performances are demonstrated in this chapter. The tuning of the temperature controller steps to set various desired temperatures and how the experiments as a whole were conducted are presented in this chapter.

Chapter 5 –Test Results and Discussions

The test results accumulated are demonstrated and discussed. The optimal PID parameters of the chamber are presented in this chapter.

Chapter 6 – Conclusions

This chapter concludes on the accumulated results that were achieved and recommendations are then made for potential future work.

CHAPTER 2
LITERATURE REVIEW

This chapter comprises of the reviewed literature related to this study. A brief background on furnaces distinguishing the difference between laboratory and industrial furnaces are presented. The major differences that these types of furnaces have are discussed. The uniaxial and biaxial tensile tests are described. The elevated temperature testing of smart materials including shape memory alloys is being reviewed.

2.1 FURNACES

A furnace is a thermally controlled chamber device that generates extremely high temperatures which is mostly used in the industrial sector for commercial production. There are furnaces on the contrary that do not operate at extremely high temperatures, furnaces like laboratory furnaces. Unlike industrial furnaces, laboratory furnaces are designed for experimental and research purposes, they usually come in moderate sizes and are electrically powered. Literature shows that laboratory furnaces operating temperatures are up to 1500^{o}C. Industrial furnaces operates at temperature of higher than 1600^{o}C (Motzfeldt, 2013 and Vert, 2016).

Dolezal (1967) describes, furnaces as systems that undoubtedly require an application of the fundamental laws of thermodynamics. According to Dolezal, there are two thermal processes that simultaneously take place in all furnaces and these are based on using the thermodynamics laws. These processes are the radiation of the heat from the energy source and the partial heat transfer of this energy through the wall thickness of a furnace. Further discussions on these thermal processes are reviewed later in this section.

There are many different types of thermal chambers. Their difference is based on various factors, a few amongst the many is according to the source of heat that drives them, the industry that they are used in or products that they provide heat to, and the temperature range they are designed to operate at (Mullinger & Jenkins, 2013; Bockris, White & Motzfeldt, 1959; Halvorsen et al., 2016 and Han et al., 2016).

Mullinger and Jenkins further explained that, when designing furnaces there are two major phases that has to be catered for, that are the process design and the mechanical design phase.

The process design is basically the design of thermal transfer and the balancing of the heat energy that circulates in the chamber. This process design phase can be achieved by performing manual

calculations, simulation using various complex computerized systems and mathematical models, all these processes are based on the thermodynamics equations and this is confirmed by the work reported in the literature (Ghobara, 2013 and Halvorsen et al., 2016).

According to Motzfeldt (2013), the thermodynamics equation presented in equation 1 below is associated with the balancing of heat energy using the rate of heat flow (q) through a wall thickness that has a thermal conductivity (k). In steady state conditions the heat flux is constant throughout the wall thickness of the furnace and this condition is assumed when applying this equation.

$$q = -kA\frac{dt}{dx} \quad (1)$$

A, represents the perpendicular area of the refractory wall (the insulation lining) to the heat flow and $\frac{dt}{dx}$ represents the temperature gradient across the refractory thickness.

In any thermodynamics system or thermal chamber, heat can be transferred through three distinct types of medium. These are the conduction, convection and radiation heat transfer subsequently described below.

Conduction heat transfer, virtually takes place primarily between solid materials of different temperature gradient. A cool object in direct contact with the one that is hot will be heated by the warmer object, causing the cooler object to increase its temperature until they both reach the state of equilibrium (Simonson, 1975).

Convection heat transfer, is the transfer of heat from a solid material into a liquid or air or any fluid media that is in motion provided that there is a temperature difference between the two. This phenomenon of fluid particles in circular motion can either be natural convection or forced convection. Natural convection is said to be induced by the natural transfer of heat and forced convections are induced by external forces imposed on the system (Janna, 2011).

Radiation heat transfer, takes place in electromagnetic waves. These waves are transferred from an origin of high energy through space to the work piece. It is the fastest form of heat transfer when compared to the other two (Cengel and Boles, 2008).

These three types of heat transfer methods can either be at transient or at steady state condition in a system. These two conditions determine the behaviour of a thermal system over a period of time. Generally, the transient conditions are found at the beginning and sometimes at the end of the steady state conditions (Simonson, 1975). Transient conditions imply unsteady conditions and steady implies that the system is constant and there are no changes or disturbances in it over a certain period of time (Cengel and Boles, 2008). It is also found that in steady state conditions the input energy is balanced with that of the surroundings resulting in constant temperature of the thermal systems (Motzfeldt,

2013). Reaching steady state conditions at a faster rate is usually ideal but this depends on the desired system behaviour. However, the time taken by the system to reach the steady state can determine the system efficiency relative to the desired output. Figure 2.1 illustrate the graphic output of the transient phase and how it can be controlled. Comparing curve (a) and (b), (b) reaches final value at a delayed rate and (a) has reduced the time it took the system to reach the desired output (or the final value) at the expense of unsteady conditions and overshooting at the beginning of operation and also a delayed stability phase. Venturini et al., (2015) also confirms that unsteady condition should be taken into consideration when the study was conducted on the pellet stove.

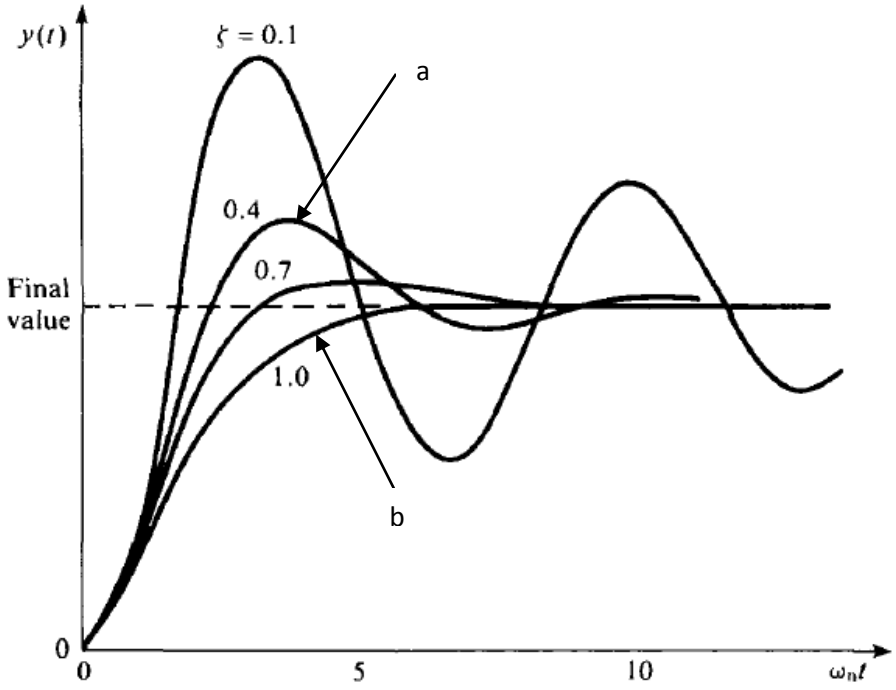

Figure 2.1: Variation of transient response with damping ratio

(Warwick, 1996)

As previously mentioned that in thermal chambers heat is transferred differently from the heat source to the work piece (or samples) inside the chamber depending on the type of furnace, the method of heating or the type of heat source. Heat source in a furnace can either be a nuclear, chemical or electrical heat source indicated by Mullinger and Jenkins (2013).

Electrically powered furnaces are better to control as compared to other types of laboratory furnaces according to Bockris, White and Motzfeldt (1959). The laboratory furnaces are grouped into two the electric arc furnace (EAF) and electric resistance furnace. These furnaces are well known for their good power efficiency (Lynon et al., 1914).

In electric resistance furnaces, the heat source is from a solid resistor, this form of heating can be justified in two ways one being conduction heating if the work piece in the chamber is in direct contact with the resistor. Another form of resistance heating is through radiation of heat from the resistor into the air of the chamber, the resistor and the work piece are not in direct contact.

The mechanical designs are the detailed drawings prepared for manufacturing and assembling of the actual physical furnace. Furnaces have common components which are an insulation lining, a source of heat and a temperature controller according to Mullinger and Jenkins (2013). These three components are technically represented in drawings as a guide to manufacturing and assembling of the furnace to be built. The insulation lining better described as the refractory lining is discussed below based on the literature and studies previously conducted on various types of furnaces currently available.

2.1.1 Refractory linings

According to Vert (2016), it is challenging to design or select a perfect refractory lining but an optimal one is possible. Ceramic materials are the dominantly used materials in furnace as an insulation lining which are better known as a refractory lining. Refractory bricks used to build these linings are formed using various different composites to suit the intended application (Scheunis et al., 2015). A ceramic refractory lining is built from ceramic fire bricks that are moulded using granules of different sizes of ceramic composite materials. The granule size defines the porosity property, which is later explained under refractory properties. These linings can be single or multi-layered walls to serve as an insulator or a wall preventing the heat generated in the heat chamber from escaping to the surroundings. Refractory linings have different chemical compositions which explains their classification that assists in appropriately assigning them to the relevant application Refractory Lining (2010).

When designing a refractory lining it should ensure the system to have the minimal heat losses as possible because, unmanaged heat losses can be financially costly and lower the integrity of the system especially in industrial furnaces. According to Motzfeldt (2013), on the contrary, for laboratory furnaces power cost is not a critical issue when designing them. One can design refractory linings in two forms one made of firebricks and the other made of monolithic modules.

Most refractory linings are made of firebricks due to them being cost effective when compared to monolithic modules. However, when comparing the efficiency of monolithic module lining to that of firebricks, monolithic modules are ideal but with high costs defects. Kanthal Manufacturers have designed a patent the prefabricated monolithic lining called a *fibrothal* refractory. These *fibrothal*

modules come in various sizes and shapes to suit designers' needs, especially for systems that do not compromise heat losses. What makes monolithic modules ideal is that they are readily formed into the shapes or chambers of desire; this reduces the number of joints in the insulation lining also reducing the heat losses in that particular system it's used in (Kanthal, n.d.).

2.1.2 Refractory properties

Refractories are important components when designing an efficient furnace because they trap the heat radiated to the work piece in the chamber (Samuelsson, 2017) hence, why an optimal refractory is needed. Determining an optimal refractory for a desired application can be done by identifying the relevant properties that the desired refractory should have. There are many physical and chemical properties of refractories, amongst them are apparent porosity, thermal conductivity, thermal expansion and refractoriness. These properties are subsequently discussed.

The apparent porosity factor is a ratio of open pores volume to the total volume of the refractory. The pores of refractories are a result of the space in-between the moulded granules. This property is important in all furnace designs, Karadeniz et al., (2007) reported that if the temperature within the chamber is fired onto the refractory wall it eventually causes the apparent porosity to decrease as a result the granules melt causing a less efficient refractory (see Figure 2.2) Lyon et al., (1914) also had previously discovered that an over powered furnace is short lived, as a result of a damaged refractory wall.

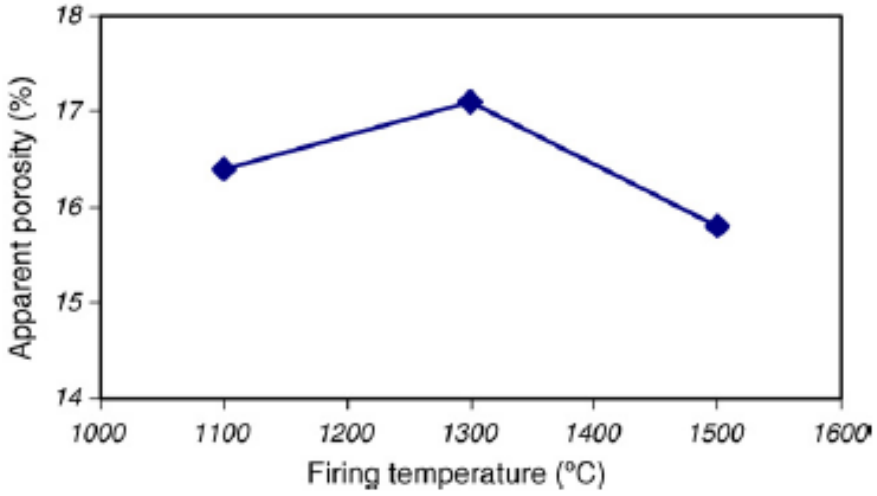

Figure 2.2: Effect of firing temperature to the refractory's apparent porosity for 0.23 n-value (Karadeniz et al., 2007)

Porosity is inversely proportional to the thermal conductivity of the refractory. In a system to achieve a low thermal conductivity the refractory must have high porosity this assists in keeping heat losses at

a minimal. A study conducted by Shimizu et al., (2013) showed that a high porosity aluminium refractory brick was attainable with the aid of GS (gelation of slurry) a method of producing high ceramic foam; when they lowered the thermal conductivity of the aluminium refractory brick they achieved results porosity of 90 to 97.5 %.

Thermal insulators are those materials that do not conduct or are poor conductors of heat with very low thermal conductivity as compared to conductors of heat. The thermal conductivity property is a coefficient that determines the heat lost or gained in the insulated system. As previously implied that, if the thermal conductivity is low then it means the porosity of the refractory is high. Zivcová et al., (2009) also demonstrated that there is a relationship between porosity and thermal conductivity for certain composites. This property is also dependent on the thickness of the refractory owing to the temperature gradient across the thickness. Akiyoshi et al., (2017) demonstrated mathematically that for insulating refractories the thermal conductivity increased as the temperature increased (see Figure 2.3).

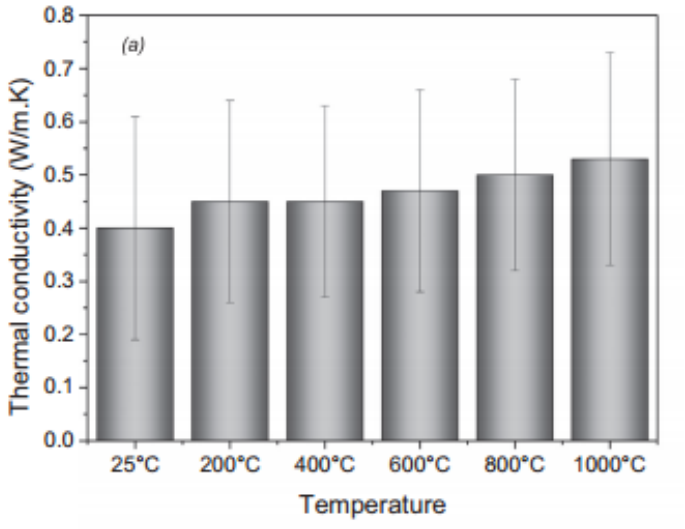

Figure 2.3: Mean thermal conductivity (k) values with temperature measured for the: (a) insulating pre-fired at 1000 °C for 5 h

(Akiyoshi et al., 2017)

Thermal expansion property is a coefficient that determines the rate of expansion or contraction of a material under thermal loading. Knowing this thermo-mechanical property is very important especially for materials operating at high temperatures.

The coefficient of thermal expansion can either be presented as permanent linear change or reversible expansion of a material depending on the insulation material composition structure explained in Zuda and Cerny (2009) work, which is a result of the change in temperature imposed on the material as defined by Harbison-Walker, (2017).

Studies have been conducted investigating various composite materials coefficient of thermal expansion at various temperature ranges. Theoretically thermal linear expansion coefficient is directly proportional to the thermal load. However, Zuda and Cerny (2009), demonstrated that the thermal expansion of the reviewed materials was not constantly directly proportional to temperature. They showed the quartz sand and electrical porcelain aggregates had an impact on the thermo-mechanical behaviour of alkali-activate aluminosilicate composite illustrated on Figure 2.4. The first aluminosilicate composite had aggregate of quartz sand shown as NS and the other aluminosilicate composite aggregate was electrical porcelain shown as EP on the figure below where it is illustrated that thermal expansion increases with temperature but eventually drops with the further rise in temperature for the two aluminosilicates.

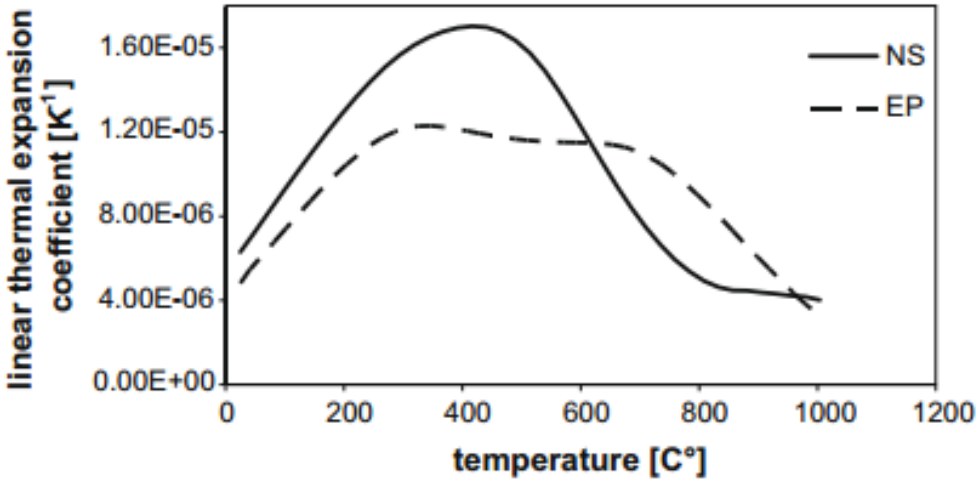

Figure 2.4: Linear thermal expansion coefficient of analysed materials as function of temperature (Zuda and Cerny, 2009)

The melting point (or refractoriness) of a refractory material is an important thermo-mechanical property of refractory materials used in industrial furnaces more especially. The melting point temperature of the selected refractory contributes to the safety of personnel and other equipment in the plant or laboratory. This property can be used to determine the optimal refractory by selecting a refractory that has a melting point temperature higher than the maximum temperature that the system will experience or operate in, says Motzfeldt (2013). The aggregate or granule compounds that are used to form refractories usually have high melting points. The melting point temperatures of these pure compounds can be used to determine the desired refractory based on the presented Table 2.1.

Table 2.1: Melting points of pure compounds

(Energy Managers and Energy Auditors, n.d.)

Pure compound	Formula	Melting Temperature ^{o}C
Alumina	A_2O_3	2050
Lime	CaO	2570
Chromite	$FeOCr_2O_3$	2180
Chromium Oxide	Cr_2O_2	2275
Megnesia	MgO	2800
Silica	SiO_2	1715
Titania	TiO_2	1850

2.2 PROCESS CONTROL SYSTEMS

After the mechanical system has been designed and manufactured an additional system to monitor and control is required. With the advancing technology control engineers had emerged in making this possible. Proper process control is an important feature in any system. The primary motive of having process control is for safety, the ease to monitor a system and economic reasons, especially for industrial systems where personnel and profit are at heart of the organisation. According to Warwick (1996), in 1934 Hazen published "Theory of servomechanisms" where the first use of the term 'servomechanism' which then became a descriptive term for many feedback control systems.

There are two fundamental ways of analysing a control system which are modelling and designing the control system, (Warwick, 1996). Designing a control system is comprehendible, if the desired output is preliminary defined- performance wise. However, the design of the system is dependent on the model of the control system. Block diagram represents the components of a closed or open loop system as illustrated on Figure 2.5 but in an open loop system there is no feedback from the system output, hence it is an open loop system.

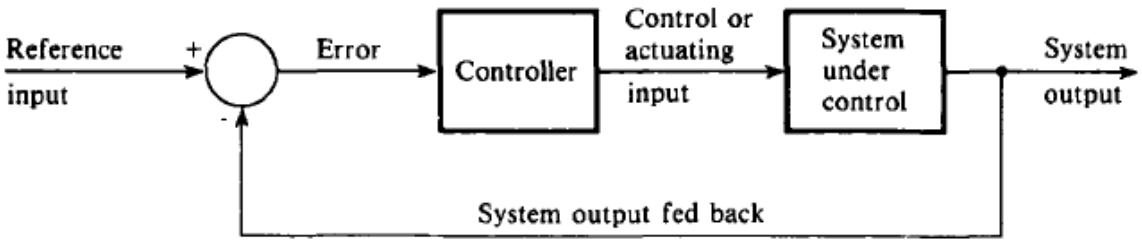

Figure 2.5: Closed-loop system of the control system

(Warwick, 1996)

A closed loop system is more accurate and stable when compared to an open loop system. Gan et. al., (2017) studied a full closed-loop system where the micro-vision system (MVS) was used to obtain feedback signals in place of using traditional displacement sensors to improve the positioning accuracy of a micro/nano positioning system. The findings demonstrated one of the benefits of successfully using the closed loop system.

2.2.1 Process controller tuning

Process control is vital for simple and complex system. A controller device configuration (or tuning) determines the degree of the control over a system. There are many types of tuning methods amongst the many are: Zieglar-Nichols tuning, Cohen-Coon tuning, Matlab tuning and the manual or empirical tuning method. All these approach use the proportional, integral or the derivative gain to adjust the parameters on the control device, as a combination of all or some of these gains to control systems. When adjusting any of these three parameters it is reflected on the behaviour of the system that is being controlled. This can be monitored visually or logged using data loggers that represent the systems behaviour graphically as illustrated on the Figure 2.6.

A controlled system has two different phases that it under goes before reaching the desired output. Firstly, it goes through the transient phase which is the early stages of the system. Secondly, it goes through the steady state conditions where the system stabilises and where there is little or no changes occurring in it.

When tuning the parameters to control a system the parameters can be of moderate tuning or aggressive tuning which can respectively result in a slow or fast system response as illustrated on Figure 2.6 below. In the moderate tuning it is seen that the system takes longer to reach the set point and spending too less time being stable this makes it suitable for systems that do not compromise overshooting. In the aggressive tuning in the transient phase the system aggressively reaches the set point and sometime even overshooting as a result affects the steady state conditions. However, the aggressive tuning yield longer steady state conditions but it is not desirable for systems that do not compromise overshooting. (Control Guru, n.d. and Skogestad, 2001)

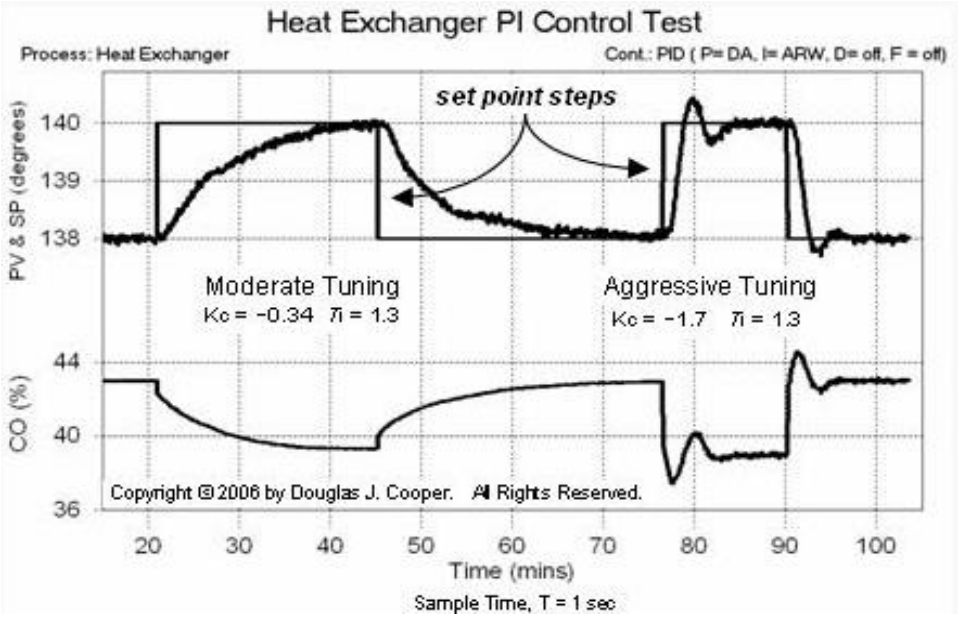

Figure 2.6: Heat Exchanger PI Control Test

(Control Guru, n.d.)

There are four types of proportional integral derivative (PID) controller variations namely the P, PI, PD and PID. According to Temel et al., (2013) in almost all cases fast transient response and zero steady state error is desired in closed loop systems. This supports what is demonstrated in Figure 2.6 where steady state conditions at set value was achieved for the aggressive tuning. A proportional (P) system's fundamental purpose is to energize the system so that the set value (sv) is reached by eliminating the error between the sp and process value (pv). However, it will not always 100% eliminate it. The PI system on the other hand is there as an improved version of the P system that further eliminates the steady state errors from the P system. These are mostly preferred type of controllers for first order plants. The PD system is specially to eliminate sudden disturbances that might occur in the system. PID controllers are better known as three term controllers. These controllers control the system in question using the three parameters. They are complex controllers that yield better control for two or higher order systems if compared to the P-I and P-D controllers Temel et al. (2013).

2.3 TENSILE TESTS

A tensile test is a mechanical test that determines mechanical induced properties of metallic and non-metallic materials using a tensile and compression testing machine. This test can either be a tension or a compression test depending on the direction of the applied load. These two tests are important tests that are fundamentally designed to determine the strength of material a material under review (Davis, 2004). After the strength has been determined or verified using the tensile test, the tested

materials are now ready to be assigned for certain applications (Han, 1992). This test is essential for materials engineers (and in other related engineering fields) because it simulates the material behaviour using a small sample from the actual material. The results attained from the test gives engineers an idea of how the actual material or structure will behave under certain loads. This also allows them to improve on their designs based on the outcome of the tensile tested materials. The uniaxial and biaxial tensile tests are further discussed in this section.

2.3.1 Uniaxial tensile test

According to Kutz (2013), the uniaxial tensile test is the most basic and the most performed type of tensile test. It is done to test the mechanical strength of materials. This test is set up by clamping the two ends of the specimen under review and applying a vertical load in compression or tensile direction on one end of it until it reaches its breaking point. The way a specimen is prepared and clamped has an impact on the tests result, therefore the correct alignment is important. See Figure 2.7 on how an ideal specimen is shaped like and how to correctly clamp it for a uniaxial tensile test.

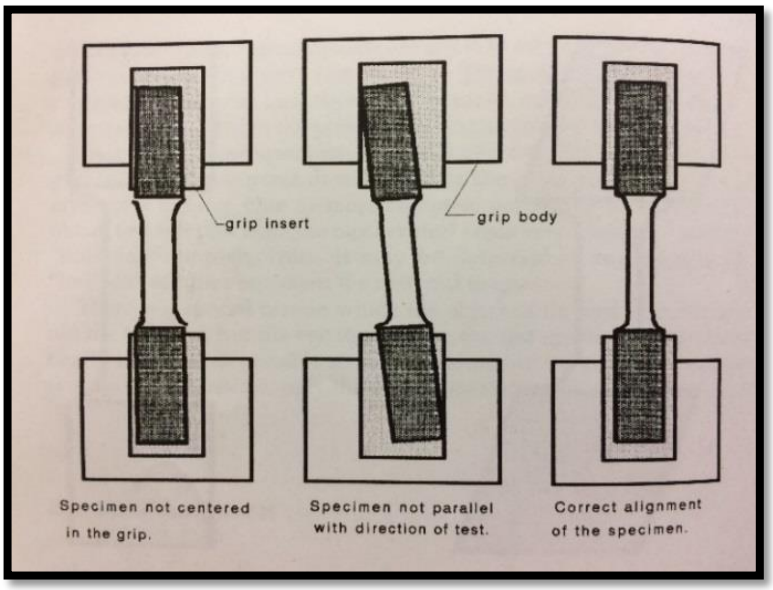

Figure 2.7: Alignment of specimen

(Han, 1992)

2.3.2 Biaxial tensile test

Biaxial tensile test is applicable to anisotropic materials. Anisotropic materials are materials that have mechanical strength in various directions or planes in the body of that material. A tensile test that will enable applying loads in multi-directions is a requirement for these materials; unlike the uniaxial

tensile test where isotropic material is assumed and the test load is single and applied in one direction. Studies show that sheet metals have mechanical strength in different directions due to the manufacturing process they undergo therefore, biaxial tensile test is highly recommendable in determining their mechanical properties (Hannon and Tiernan, 2008). Figure 2.8 illustrates a typical specimen called the cruciform specimen that is used when a performing the biaxial tensile test.

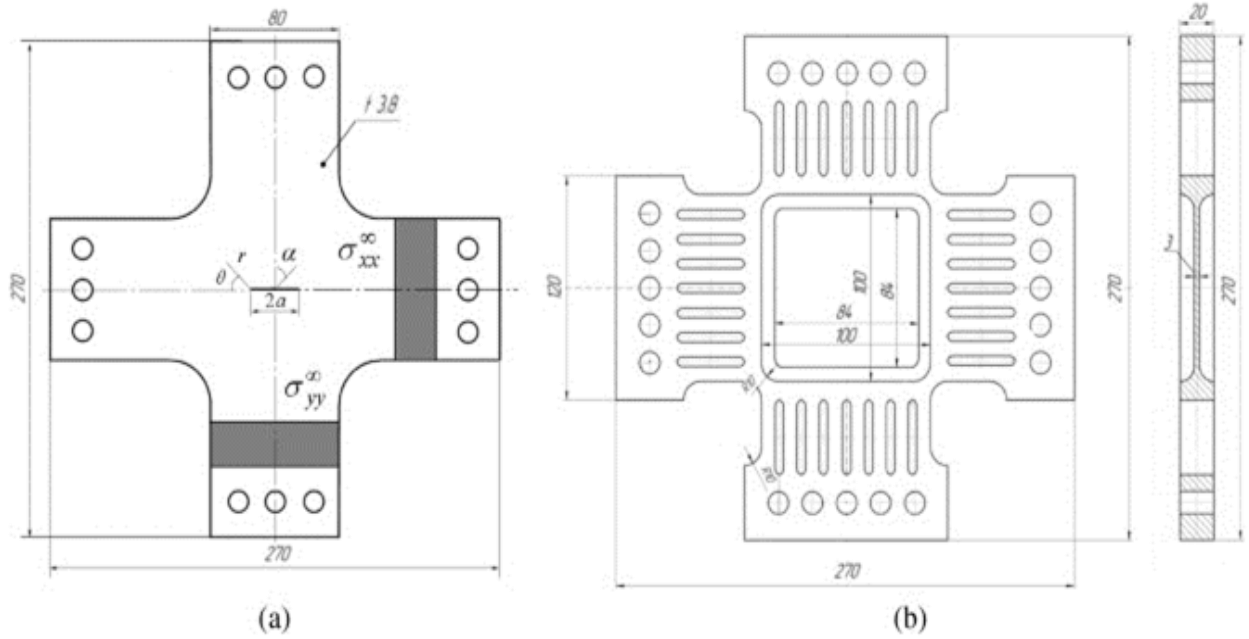

Figure 2.8: (a) Flat cruciform (CS- 1) and (b) cruciform specimen with thinning working area (CS-2) (Shlyannikov et al., 2014)

2.4 ELEVATED TEMPERATURE TESTING

Testing materials only at room temperature limits the test results yielded by a tensile testing machine. In the long run this limits the assigning of materials to various applications. Tensile testing materials at elevated temperature has recently became popular. There are materials that show special mechanical properties when tested at elevated temperatures. Therefore, exploring material behaviour at controlled high temperature ranges has become an advanced requirement for the tensile test (Mills-Brown et al., 2013).

Yarlagadda (2002) performed tensile test on Alloy HT-9 at different temperatures ranging from 100^{o}C to 600^{o}C. The results revealed that ultimate tensile test (UTS) varies with temperature. Furthermore, there are other special materials that require controlled testing called the shape memory alloys.

Shape memory alloys (SMA's) are very intricate materials that have been studied a lot recently. These smart materials have interesting properties that are exhibited at different temperature ranges, owing

to their different internal structure at those various temperature range. The two prominent properties that draw attention to these smart materials are the shape memory effect (SME) and the super elasticity (SE) (Srinivasan and McFarland, 2001). These properties are a result of the change in the internal structure of SMA's.

When an SMA material is at martensite phase, this implies that the material is exposed to a low temperature or room temperature where its microstructure has zig-zag atomic arrangement which is called twinned martensite (see Figure 2.9). When the stress is applied to the SMA, the twinned martensite is transformed to detwinned martensite. This implies that the SMA material is deformed. When the SMA is exposed to temperature above room temperature or martensitic temperature, the formation of the austenite phase start to appear (see Figure 2.9). This implies that the SMA material is gaining its original shape.

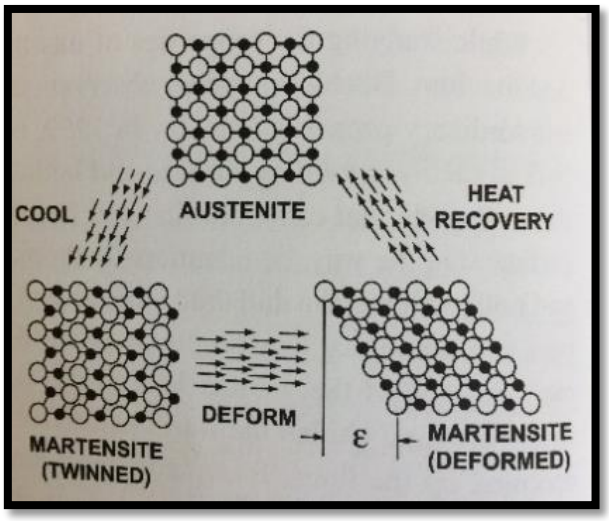

Figure 2.9: Shift in crystal structure accompanying phase change in shape memory alloys

(Srinivasan and McFarland, 2001)

Having explained and illustrated the phase change occurring at the microstructural level of SMA which is SME, this is an effect which enables SMA to regain its original shape upon thermal load. An extensive work has been done on the SME for various applications (Jiang et al., 2016 and Shivasiddaramaiah et al., 2016).

Now, on the other hand SE also known as psuedoplasticity which is the ability of an SMA to fully recover its original shape upon removal of the applied physical load. SE takes place at a temperature above austenite finish temperature. When a physical load is applied on this alloy causing it to transform phase from twinned martensite to detwinned martensite which is termed stress induced martensite (Srinivasan and McFarland, 2001). However, great amount of research has been done around the SME due the flexibility and applicability of this property in various systems.

CHAPTER 3
DESIGN AND MANUFACTURING OF CHAMBER

This chapter consists of the detailed design and all manufacturing and assembling processes used to produce the chamber. A furnace is a thermo-mechanical device that generates heat to heat the products or work piece within the heat chamber, bringing about mechanical or physical change on those items. The heating efficiency of the manufactured device depended mostly on the three major components; the heating elements, the insulation of the system (the refractory lining) and the temperature control system the proportional integral derivative (PID) controller were used in this study. The chamber that was designed and manufactured is classified as a laboratory furnace, due to its function and intended application, for it to improve the function of the previously specified tensile testing machine. In thermal systems the point of equilibrium is an important state that is yielded by systems. The control system is there to cater for different desired variations of temperature output that the end user might need in the future of performing a temperature controlled tensile test. This chapter presents the possible design to go about controlling the tensile test conditions.

3.1 CHAMBER DESIGN

The detailed design of the chamber is presented in this section. The electrical circuit is illustrated on Figure 3.1 and how the heating elements were featured on to the heating chamber. The PID controller and the solid state relay (SSR) are shown on how they are incorporated onto the system which are assembled in a specially designed control box. The insulation lining design that isolates the controlled temperature conditions from the laboratory's environmental conditions is presented in this section. This was done with an aid of the special ceramic refractory material that was selected based on the manual calculations performed. The refractory shell holder was designed for the purpose of protecting the fragile refractory lining. The shell of the chamber was constructed using mild steel angle iron and sheet metal material.

3.1.1 Electrical wiring design

When the power is switched on current flows through to the solid state relay and the PID controller to the heating elements (the load) inside the heating chamber (see Figure 3.1). There are two heating elements inside the chamber connected in series using the ceramic connectors (see (a) on Figure 3.2). There were two other electrical connectors b) brass and c) plastic that could have been used, but with

the heat that the heating elements imposed on the connection line the ceramic ones were optimal when compared to the other two illustrated on Figure 3.2. However, the plastic connectors (c) were used for connection at the nodes. The heating elements are arranged on either sides of the chamber walls so that the specimen tested is centred in between them for optimal heating see Figure 3.3.

The thermocouple (TC) keeps track of the actual temperature called the process value (PV) or actual temperature inside the chamber at all times. This temperature is reflected on the PID controller to the tenth decimal. After setting the desired value called the set value (SV) on the controller, the heating element is energized based on the configuration of the parameters to yield the desired temperature. The SSR is there as a switch to actuate current of the PV to balance it to equal to the SV and this takes place after the end-user has set or tuned the SV on the PID controller.

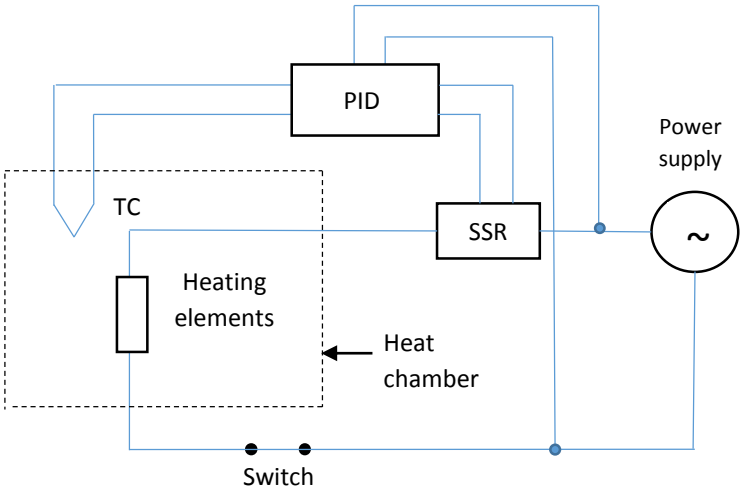

Figure 3.1: Schematic of electrical circuitry

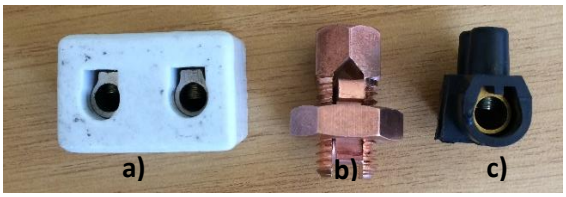

Figure 3.2: Electrical connectors

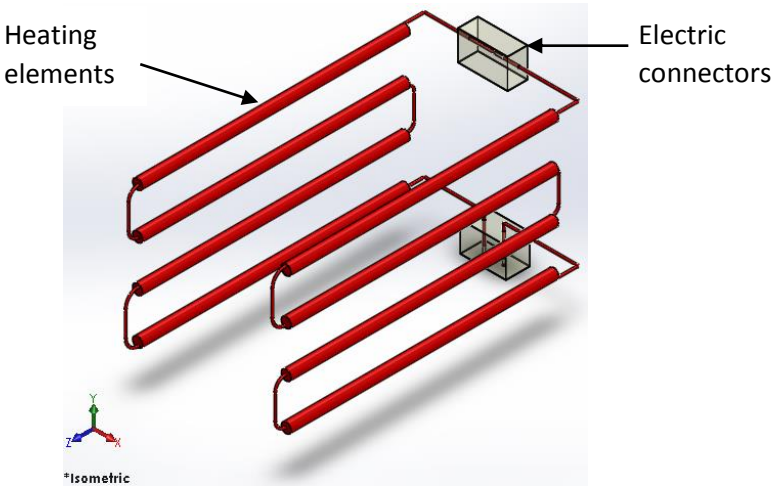

Figure 3.3: 3D Solidworks design of heating elements

After the electrical circuit had been designed, the optimal heating elements had to be selected. Looking at the first aim listed in Chapter one, the heating elements need to withstand the maximum operating temperature 350^{o}C. Possible overshooting was to be taken into consideration at this early stage. This meant that the refractory insulation should be designed to handle more than 350^{o}C. The predefined acceptable percentage overshoot initially was 500^{o}C for the design calculations purposes. However, the actual percentage overshoot is presented and discussed in detail in Chapter 5. The temperature 500^{o}C was used in designing and selecting the optimal refractory material presented in section 3.13.

3.1.2 Heating element design

The two identical heating elements were supplied by the local supplier *Industrial Alloys* (Pty) Ltd which were manufactured out of the Kanthal wire. The Kanthal wire was highly recommendable when compared to the nichrome wire. The final specifications of the wire used to manufacture the heating elements are presented in this section. Set of equations used for specifications calculations are as follows (Sachithanandam, 2015).

$$H = 5.72\ ke\left[\left(\frac{T_1}{100}\right)^4 - \left(\frac{T_2}{100}\right)^4\right] \quad W/m^2 \qquad (2)$$

H- Heat radiated (W/m^2); T_1- Heating source temperature (K); T_2- Surface to be heated temperature (K); k- Radiation efficiency; e-constant- Emissivity

$$A_{circumf.} = \pi dl \qquad (3)$$

$$C = H \times A_{circumf.} \qquad (4)$$

$$P = \frac{v^2}{R} \quad (5)$$

$$R = \frac{\rho l}{A} \quad (6)$$

$$A_{crosec.} = \pi r^2 = \frac{\pi d^2}{4} \quad (7)$$

$$\therefore\ l = \frac{v^2 d^2 \pi}{4P\rho} \ldots\ldots \quad (8)$$

$P = H\pi dl$

$$\therefore\ l = \sqrt{\frac{dv^2}{4H\rho}} \ldots\ldots \quad (9)$$

P- Power (W); v- voltage (V); R- resistance (Ω/m); ρ- resistivity (m^2/Ω); l- length (m); A- area (m^2); d- diameter (m); C- total heat dissipated

Equating equation (8) and (9) so that one can be able to determine the diameter of the optimum Kanthal wire.

In the literature reviewed in Chapter 2, it was shown that laboratory furnaces operating range is up to $1500^{O}C$ and that they are electrically powered. With this knowledge the furnace in this study is set to be a laboratory furnace reducing the scope of the type of heating elements that could be possibly used as a heat source in this study. Kanthal A1 is popular for its application in furnaces with its melting point of $1400^{o}C$. However, Kanthal AF, AE and D have a melting of 1300^{o} C (Kanthal, 2012 and Kanthal, n.d.). An assumption that the highest temperature that the chamber will reach is $500^{o}C$ was made. Due to the stated reason the Kanthal D alloy wire was selected. Further design calculations were performed to determine the optimal wire diameter and manufacturing dimensions of this alloy.

Design calculations:

k=0.51; e=0.9; $\rho=1.35x10^{-6}$

$T_1 = 800^{o}C = 1073K$; $T_2 = 400^{o}C = 673K$

Desired power rating for the system is P= 770W; hence the power for each heating element is 770/2= 385W.

$\therefore$ H= 29416 W/m^2

Using the set of previous equations the diameter of the heating element was d= 0.61 mm.

From Kanthal (2012) the Kanthal D alloys for d=0.6mm the cross sectional area is $2.83x10^{-7}m^2$.

The heating element design is presented on Figure 3.4. It was designed to have a shank length of 110mm a pitch between shanks of 20mm. The wounding diameter was 5mm diameter. The additional wire was not wounded as for it was there to join the four shanks that were designed to produce heat in the chamber.

Figure 3.4: Schematic diagram of heating elements of the furnace

3.1.3 Refractory lining design

A fibrothal monolithic module is the most efficient means of refractory lining thus far invented. However, due to the fibrothal module being very expensive the insulation lining was made of refractory bricks. This meant that heat losses were to be expected in the system due to the weakness at the joints that is a result of physically joining the insulation bricks.

The calculations performed were to determine the optimal refractory brick by selecting the one with an ideal coefficient of thermal conductivity that would not yield the insulation lining to reach its melting point; also protecting the personnel from being exposed to the high temperature from the heat chamber. However, the most important temperature is the RUL (Refractory under load) of the refractory; which is the temperature at which the refractory will just begin to deform. In this section are the set of equations used to determine the optimum refractory. The thermal resistance approach is an electrical analogy approach, this analogy is used to determine the desired refractory. There are other available approaches like energy balance equation for conduction and heat balance over the wall thickness of the refractory to select an optimal insulation lining. (Holman, 2010)

$$Q = \frac{\Delta T}{R_T} = \frac{T_i - T_o}{\frac{1}{h_i A} + \frac{\Delta x}{kA} + \frac{1}{h_o A}} \quad (11)$$

$$R_T = \frac{\Delta x}{kA} \quad (12)$$

$$\text{Convective resistance} = \frac{1}{h_i A} \ \& \ \frac{1}{h_o A} \quad (13)$$

$$Q = h_i A(T_i - T_1) = -kA\frac{T_2 - T_1}{\Delta x} = h_o A(T_2 - T_0) \quad (14)$$

$$q = -k\,(T_i - T_o) = \frac{T_i - T_o}{\frac{\Delta x}{kA}} \qquad (15)$$

Q- Heat flow; k- coefficient of W/mK; h_x= heat transfer coefficient W/m^{2}K; q-heat flux per unit area W/m^2; A-perpendicular area to the heat flow m^2; T- temperature K.

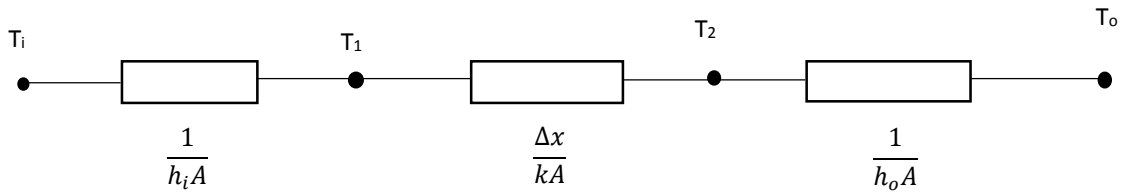

Figure 3.5: Equivalent electric circuit of heat flow across the wall thickness

Assumptions:

a) One dimensional heat flow;
b) steady state condition assumptions;
c) heat flows through the adjacent four walls (the door and back of the refractory lining were ignored);
d) One layer of refractory lining to be used of equal thickness in all 4 walls.

The initially assumed heating elements maximum temperature was 500^{o}C it was then reduced to 355^{o}C when taking into consideration the short duration of the overshoot.

Table 3.1: Data for refractory lining design

Variable	T_i (K)	T_o (K)	T_1 (K)	h_i (W/m^{2}K)	h_o(W/m^{2}K)	k (W/mK)	A_1=A_3(m^2)	A_2=A_4(m^2)
Value	628	313	664	100	25	0.17	13.68x10^{-3}	9.6x10^{-3}

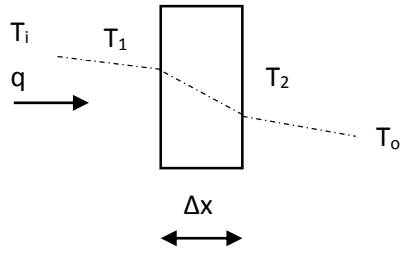

Figure 3.6: Free-body diagram of heat flow through the wall of the furnace

Therefore,

Variable	Value
q	73.1 W/m
Q	47.88 W
Δx	75 mm
T_2	55 ^oC

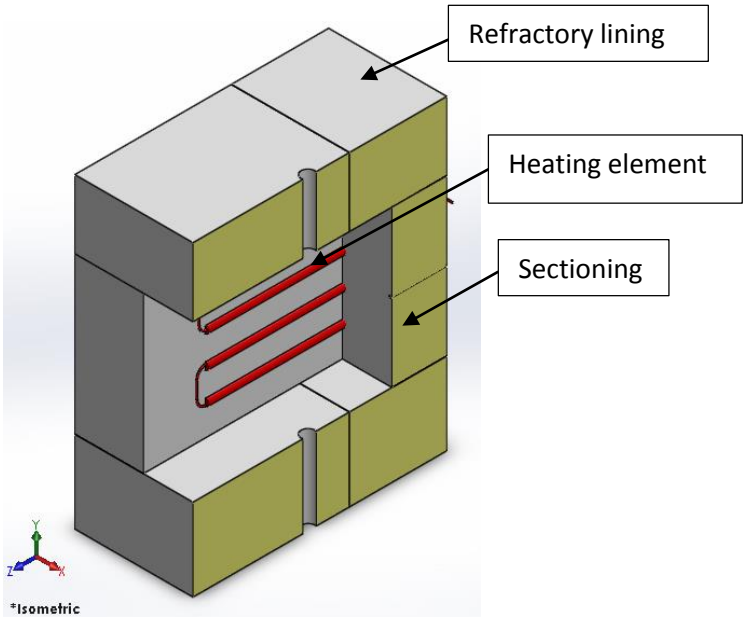

Figure 3.7: Solidworks 3D section view of refractory lining

The material that was on the insulation lining was also used in the door insulation that was supported and protected by the external mild steel frame presented in the later section. Therefore, the selected refractory material specification is the JM23 energy saving brick which was purchased from the local supplier using the design calculations as a guide.

3.1.4 Refractory shell holder design

The insulation lining has a very fragile material hence; a protective shell was necessary. Initially there were two options of materials that the shell could have been made of, namely, aluminium and mild steel. The shell structure design is illustrated on Figure 3.8 which includes the final shell of the door design. Due to the following reasons mild steel was selected over aluminium for manufacturing the shell structure.

a) Welding mild steel is more economical feasible than other aluminium joining processes available. All the welding equipment were readily available at the CPUT's Mechanical Engineering Department.

b) Due to the environment that the chamber will operate in, this will expose the chamber to vibrations which will require a solid and stable structure that will keep the machine stable and intact. Therefore, aluminium can be optimal only for a certain short period of time and when exposed to high temperature it would be more likely to fail as compared to a mild steel structure.

c) The temperature of the selected heating elements can go up to 1300^{o}C even though the chamber is designed for a maximum set temperature 350^{o}C and a maximum temperature of 355^{o}C to 500^{O}C for overshoot cases. Should there be leakages or fault in the control system aluminium material has a lower melting point as compared to that of mild steel.

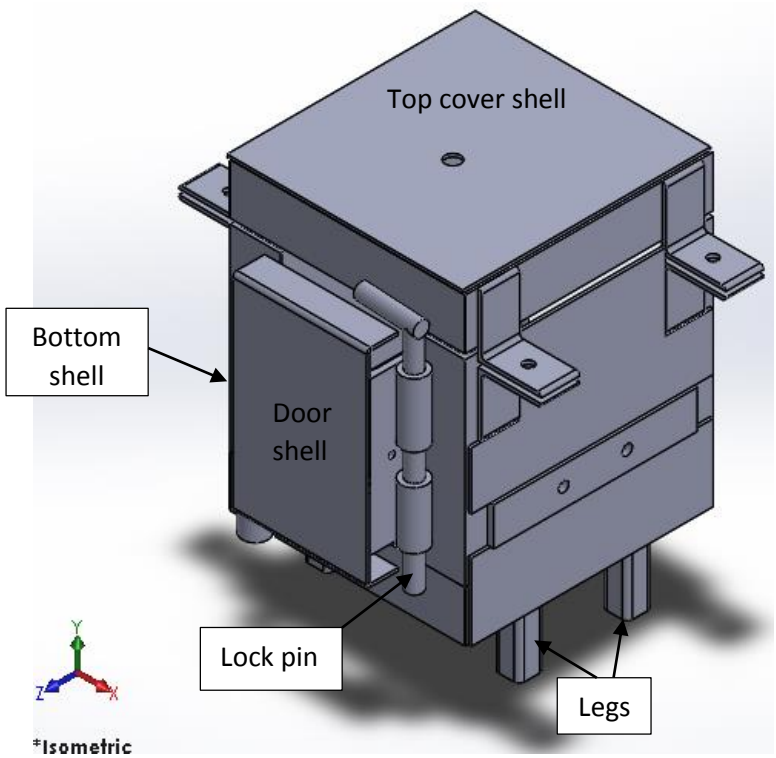

Figure 3.8: Solidworks 3D refractory shell

3.1.5 Chamber door design

Initially there were two door conceptual designs of the door. These were developed to the final presented design. The same material as that of the chamber was used to manufacture the door due to the same stated reasons above. The conceptual designs of the door were removable doors. This was developed by introducing hinges and the lock pin mechanism to seal the chamber, so that the door is

not detachable from the chamber reducing loose parts of the chamber. The detailed manufacturing drawing is presented of the door on Appendix A.

3.2 CHAMBER MANUFACTURING AND ASSEMBLYING PROCESSES

All the equipment and processes that were used to manufacture and assemble the chamber were those that were then available at the CPUTs Mechanical Engineering Department. This section presents all the necessary processes that were used to build the previously presented designs. Intricate processes were outsourced and those processes that could not be executed at the CPUT's facilities. A short brief is given on the outsourced processes that were purchased from the local suppliers.

3.2.1 Control box

The control box was manufactured out of wood because this was good electrical insulation for the solid state relay (SSR). This eliminated the use of the heat sink for the SSR. The SSR was bolted directly on to the control box back plate. The control box was then attached on to the frame holder with two M8x 100 bolts to keep it attached to the chamber. The control box was painted with black acrylic paint. It was fixed on the shell first before the refractory lining was inserted inside the shell. However, the assembling of the control box was first completed separately and then attached to the shell using the two bolts, washers and nuts. See Figure A1 on Appendix A.

3.2.2 Heating element

The selected wire size that was used to prepare the wounded heating element. Figure 3.4 was the guideline as to how the shape of the heating element should be and the length of the wounding. The supply of the Kanthal wire and the manufacturing process of the heating element were outsourced *Industrial Alloys*. The job preparation of the elements was generated based on the design that was supplied to prepare the wire into the wounded heating element.

3.2.3 Refractory lining

The refractory lining is a very light weight and chalky material. Machining of this material was done by filing off the unwanted material, to remove large amounts of materials a wood hack saw or a bustard file was used and then for precise detailing a fine file was used. Where drilling was necessary low speed was used to protect the refractory from chipping and cracking. When drilling this material clamping it to the vice was carefully done because if too much pressure was applied the refractory cracked especially for thin profiles. Therefore, the handling of this material was delicate when machining it down to size. The grooves for the heating elements were filed using the fine square profile file. Holes were step drilled to size to protect the brick from cracking.

3.2.4 Shell coating- Powder coating

The powder coating process was used to coat the outside of the shell, for the shell protection and ergonomics purposes. This process was outsourced from the local supplier *M & S Epoxy Powder Coating.* The shell was coated only on the outside because on the inside of the shell the refractory material must perfectly fit in there and the epoxy coating wound add a thickness layer that would cause the refractory material to not fit. This would cause it to be machined down which will result in a reduced insulation lining which will increase the rate of heat transfer to the outside of the chamber making it unsafe for the personnel.

3.3 FINAL CHAMBER

The final chamber illustrated on Figure 3.9 is attached onto the tensile testing machine as illustrated on Figure 3.10. The specimen connectors are first connected to the grips of the tensile tester. Then the chamber is attached allowing the bottom connector to go through the bottom hole of and into the chamber. The specimen is then clamped at the bottom connector. Now the top actuator of the tensile machine is brought down, bringing the specimen connector through the top hole of the chamber. The top end of the specimen is then clamped to the top connector that is gripped by the tensile tester's top grip. The connectors and the specimen are all within the chamber.

When the clamping of the wire specimen is secured the chamber is then plugged and switched on and the desired temperature is set. After the temperature has stabilized which is displayed on the PID controller the PV and SV are equal and not varying, then the tensile test is performed under controlled

temperature. The maximum effective length of SMA wire that the chamber can test is 85mm, and any length below that to protect the roof of the chamber from distraction when the specimen has failed. The locking bolt and nut that clamp the specimen to the connector are the reason for this possible failure.

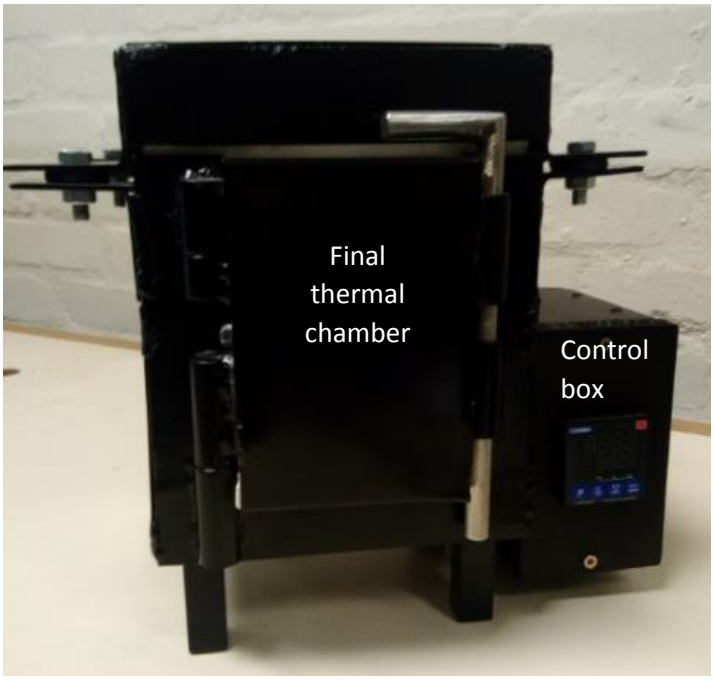

Figure 3.9: Thermally controlled chamber

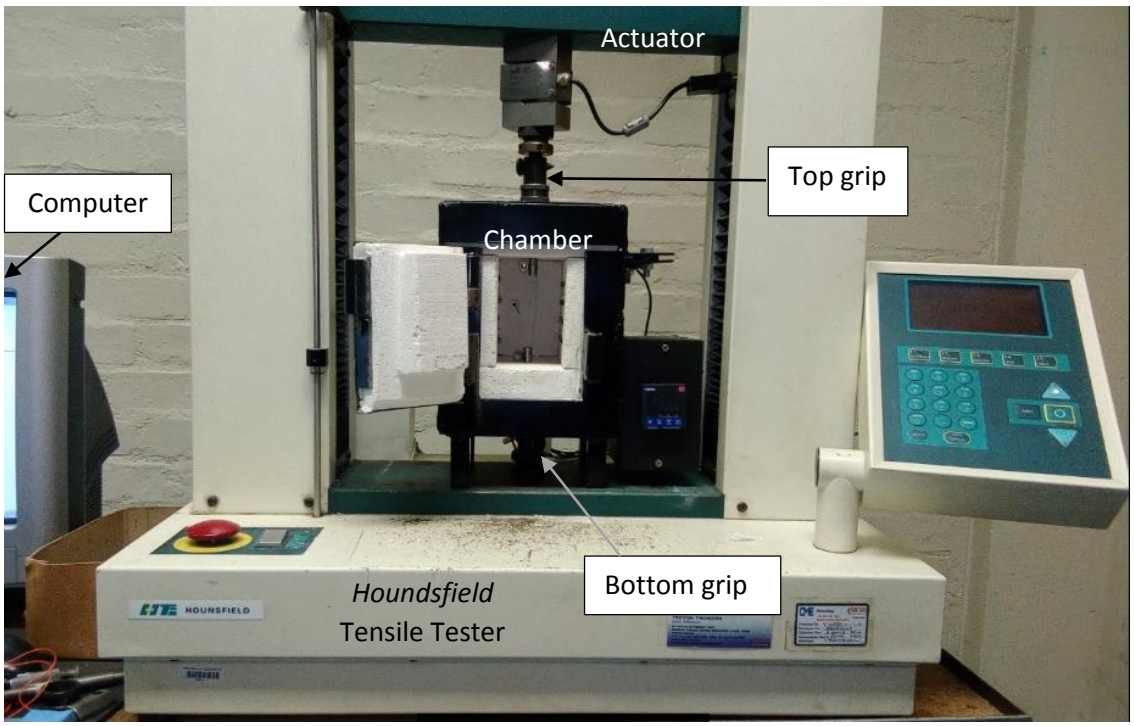

Figure 3.10: Chamber attached on the tensile tester

3.4 SPECIMEN CONNECTOR DESIGN

The challenge of having the specimen fully imbedded inside the chamber was solved by designing the specimen connectors. Also putting the grips of the tensile machine inside the chamber was not the best solution because of the size of the chamber and temperature that these parts would be exposed to. This design was an addition to the main design of the chamber. However, the material selection was not ideal as for mild steel was used for these connectors. Hence, the controlled tensile testing that was performed in Chapter 5 was done at 70^{o}C maximum. Future works will improve on the material selection for this specimen. Below are the two conceptual designs and the finally developed design of the specimen connectors. The detailed manufacturing design is presented on Appendix A. These connectors were designed so that they could fit onto the grips of the tensile machine.

3.5 SPECIMEN CONNECTOR MANUFACTURING

The bottom and top specimen connectors were manufactured on the lathe machine using the turning process. A 20mm diameter mild steel rod was machined down to the designed specifications. The 2mm diameter hole was drilled on the bench drill. Both these connectors have the same diameters but differ in the shank length as seen on Figure 3.11 and 3.12. After the connectors had been prepared they were

clamped on to the grips of the tensile testing machine and connected to the specimen wire as illustrated below. In the testing section in the next chapter, it is demonstrated how the whole set up is assembled onto the chamber for the actual control tensile test.

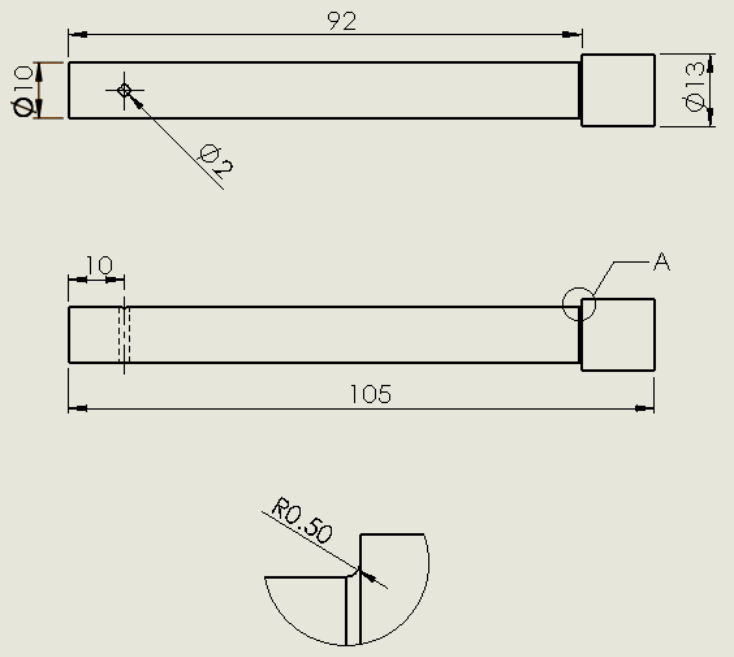

Figure 3.11: Schematic of the bottom specimen connector

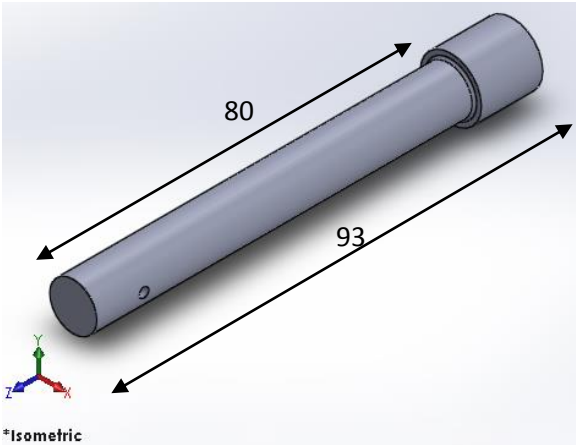

Figure 3.12: Solidworks 3D design of the top specimen connector

CHAPTER 4
EXPERIMENTAL PERFORMANCE

In this chapter the layout of the experimental preparation and procedure that were followed are presented. This work focuses on controlling the temperature of the manufactured chamber with an aid of a proportional integral derivative (PID) controller. The tests were performed to investigate the behaviour exhibited by the system when the three parameters were varied. This was experimentally achieved, by finding the ideal PID parameters suitable for the specimen of the shape memory alloy that was initially the benchmark of the study. The testing of the chamber was also attached on the tensile testing machine to demonstrate the installation setup of the specimen within the chamber. All tests were performed in the laboratory environment conditions where the chamber will be operating.

4.1 EXPERMENTAL PERFORMANCE 1: PID TUNING

After designing and manufacturing of the chamber had been completed, testing of the chamber was done. The testing stage was mainly focusing on adjusting the PID controller. Various combinations were explored until the system yielded the ideal response and those set values were concluded as the optimal parameters that the chamber will operate with. The tuning was experimentally explored and Lynch (2015) refers to it as empirical gain tuning which is also known as manual tuning. This type of tuning is not mathematically modelled but rather is based on relatively adjusting the parameters to yield the desirable system response. The temperature-time data was logged using *Explorer GLX* data logger.

In Chapter 1 under objectives it was stated that the chamber must reach the set point in the shortest possible time ideally within 10 minutes. The presented apparatus and procedure was followed in testing the chamber in pursuit for the ideal parameter. It should be kept in mind that the presented steps took place after the heat chamber had been manufactured, the holding structure was not yet necessary at that stage. However, at this point the door of the chamber was still temporary but the chamber was testable in the condition on Figure 4.1. The thickness of the temporary door was the same as that of the finally designed door so that it does not affect the dynamics of the final system.

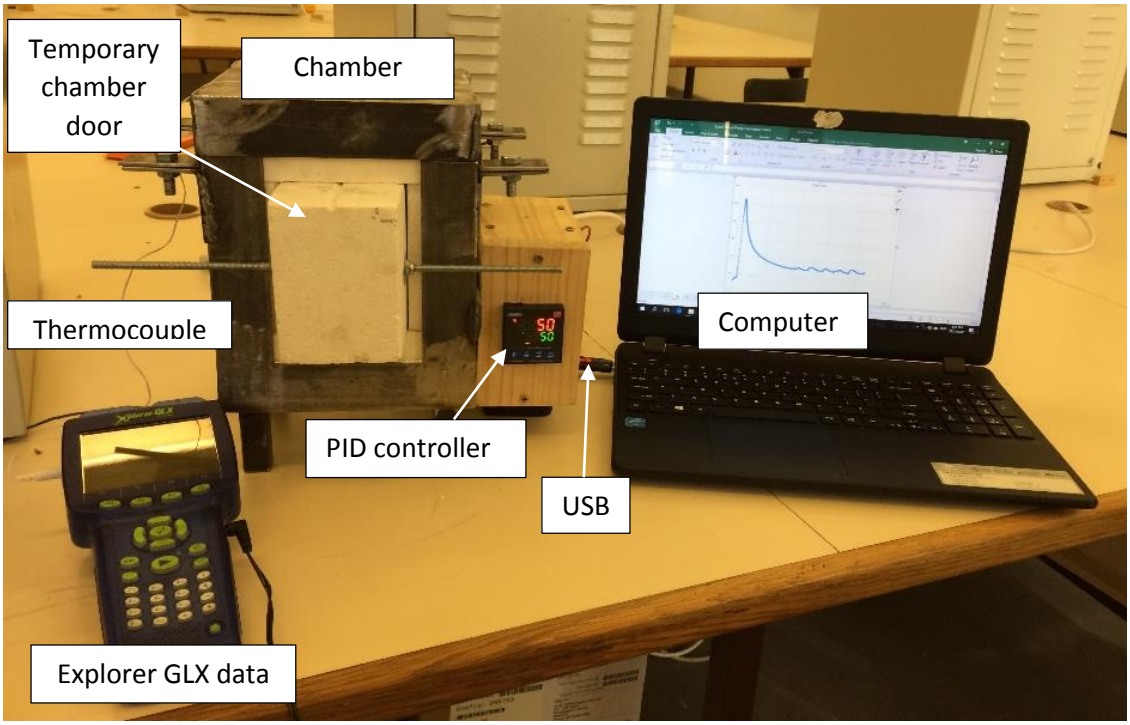

Figure 4.1: Experimental aparatus and data logging equpement

4.1.1 Testing apparatus

The following apparatus were use in performing the tests:

a) The refractory lining of the chamber which has a temporary door.
b) The *Explorer GLX* data logger with its k-type thermocouple for temperature data collection.
c) Multi-meter was tuned to temperature sensing mode to keep track if the other sensors are recording the same temperature in the chamber.
d) Multi-meter connectors with crocodile crumbs.
e) Another thermocouple connected to the multi-meter. This thermocouple was for the purpose of visually monitoring the *GLX* thermocouple data reading should its temperature readings had not corresponded to the on the PID controller and the data logger that signals a default in the system or one of the testing equipment. This also gave signal when over testing occurred, the GLX data logger would give obscure reading and unusual system behaviour.

4.1.2 Testing procedure

The *Explorer GLX* data logger's thermocouple was inserted into the chamber so that it could probe the process value (pv) or the actual temperature readings to monitor the systems behaviour. This probe was inserted through the top drilled hole of the chamber. The tip end of this probe was placed closely to the thermocouple of the chamber so that they detect the same temperature at the same location within the chamber. This probe was connected on to the temperature terminal of the data logger.

The multi-meter was tuned to the temperature sensing mode. This multi-meter was connected to the thermocouples using crocodile connectors. The thermocouple was then inserted into the chamber through the bottom hole of the chamber. Both these thermocouples were placed close as possible to the probe of the chamber but making sure that they do not contact each other as for that would give false readings see the Figure 4.2. The chamber was then closed after this was ensured.

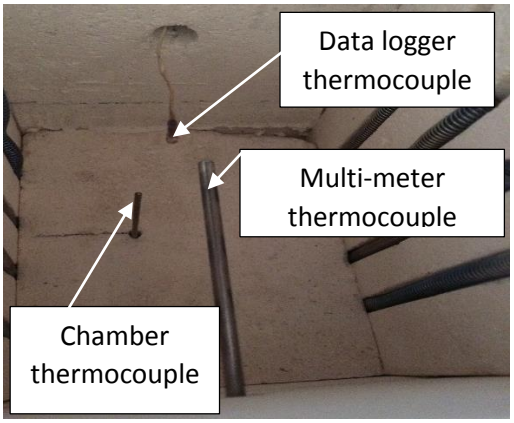

Figure 4.2: Testing thermocouple locations in the chamber

Before running the tests, a table was set out for the values that were to be used on to the controller as illustrated in Table 4.1. The chamber was switched on and these values were configured on the controller. The chamber was then switched off again after tuning the desired set of values so that the chamber cools down to below 30^{o}C and this was observed on the multi-meter.

Table 4.1: Table of test parameters at set point 50^{o}C

set	P	I	D
PID1	10	20	30

The logger was switched on and was enabled to log the data before switching on the chamber. This was done so as to record all the temperature data from the chamber. The data capturing was observed graphically on the data logger. Also, monitoring the readings on the multi-meter and the controller if they correspond to that of the data logger.

The test was running up until the set point had been reached and the steady state condition data had been captured for at least 600 seconds. The idea behind this was to check if how long logging did the system take to stabilize. The logged data was transferred to the computer for processing. This method was repeated so as to find the optimal values.

It was noted that the *Explorer GLX* data logger's thermocouple could not withstand temperature above 100^{o}C, the tests were performed using temperatures below 100^{o}C. However, few tests were performed without logging their data to test the maximum operating temperature of 350^{o}C which was successful.

4.2 EXPERIMENTAL PERFORMANCE 2: TESTING THE MAXIMUM OPERATING TEMPERATURE

The test performance at maximum operating temperature was necessary, to ensure personnel safety and practicable body temperature of the chamber. This was done to test the outside temperature T_o of the chamber the estimated temperature in the design calculations was 40^{o}C. Firstly, the set point temperature was adjusted to 350^{o}C. Then the PID 31 parameter presented on Table 5.16 in Chapter 5 were tuned. The temperature was held for 40 minutes so that true reading on the outside temperature can be recorded with the aid of the infrared thermometer so that the temperature of the outside of the chamber could be detected. The purpose of this test was to find the optimal PID values to operate the chamber at maximum temperature and to optimise the chambers outside temperature.

It was also important that a demonstration of the chamber attached onto the tensile testing machine be shown. It should be noted that designing the connectors was not part of this study. Therefore, future work may focus on designing the optimum connectors. The presented connectors were for demonstration purposes to show how the specimen will be clamped through the chamber to the tensile test machine.

The maximum height of the chamber is 114mm and the maximum that an SMA wire can extend is by 10% of its original length. Therefore, calculations were performed to design a specimen that even after it has extended to the 10% of its original length it is still within the heat chamber to avoid dissipation of heat through conduction and also to determine the maximum length of the specimen that the

chamber can take. The bottom grip of the tensile machine is designed to be stationary while the top one can move vertically up and down. The chamber was manufactured to suit this sort of movement.

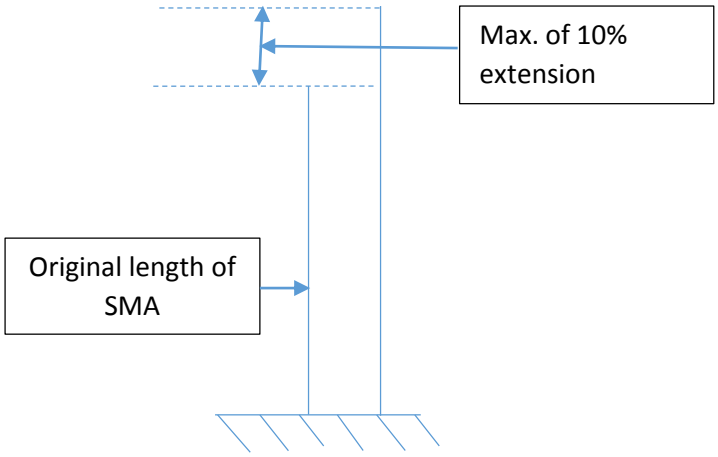

Figure 4.3: Schematics of maximum specimen connector

CHAPTER 5
TEST RESULTS AND DISSCUSSIONS

The aim of this study was to develop the temperature controlled environment of the *Houndsfield* tensile testing machine which is found at the Cape Peninsula University of Technology in the Mechanical Engineering Department workshop. This was achieved through designing and manufacturing the chamber and there after testing it. The literature reviewed in Chapter two demonstrated that conventional controllers using three term parameters have better control over systems when compared to those that have one or two control parameters. Proportional integral derivative (PID) controllers allow a maximum of three parameters control over systems. These controllers are the mostly used control devices, especially in industrial furnaces for temperature control purposes.

After the chamber was designed and manufactured, tests were conducted. The conducted tests were to examine the system response when the three parameters were adjusted. This was done so as to determine the ideal and optimal combination of PID parameters that the chamber will operate in. The behaviour of the three system parameters (P, I and D) were investigated for the closed system. The temperature-time profile was used to distinguish the system behaviour chamber.

In this chapter the results of various tested combination are presented and discussed. It was experimentally established that the proportional (P) value had an impact on the transient phase while the integral value had an impact on the steady state and the transient phases of the system. The derivative value had an impact on the transient phase which indirectly affected the steady state phase of the system. In experimenting with the three parameters, a set that yield the system to reach the set point (sp) at stable steady state in the shortest time was desired. Therefore, it was required that the impact of these three parameters be understood before concluding the ideal parameters for the designed chamber. As previously mentioned all experiments were performed at the set point temperature 50^{o}C as per reason stated in the previous chapter.

5.1 PROPORTIONAL SYSTEM

In the proportional system the integral and the derivative values were tuned to zero. Tests were performed in this sort of system at varying proportional values. The testing values for the proportional system are presented on Table 5.1. The values were tuned on the controller device for the set point of 50^{o}C (as described above) for the four tabulated sets. The behaviour that was observed is illustrated graphically on Figure 5.1.

Table 5.1: P-system parameters

Set	Parameter		
	P	I	D
P1	1	0	0
P2	10	0	0
P3	40	0	0
P4	500	0	0

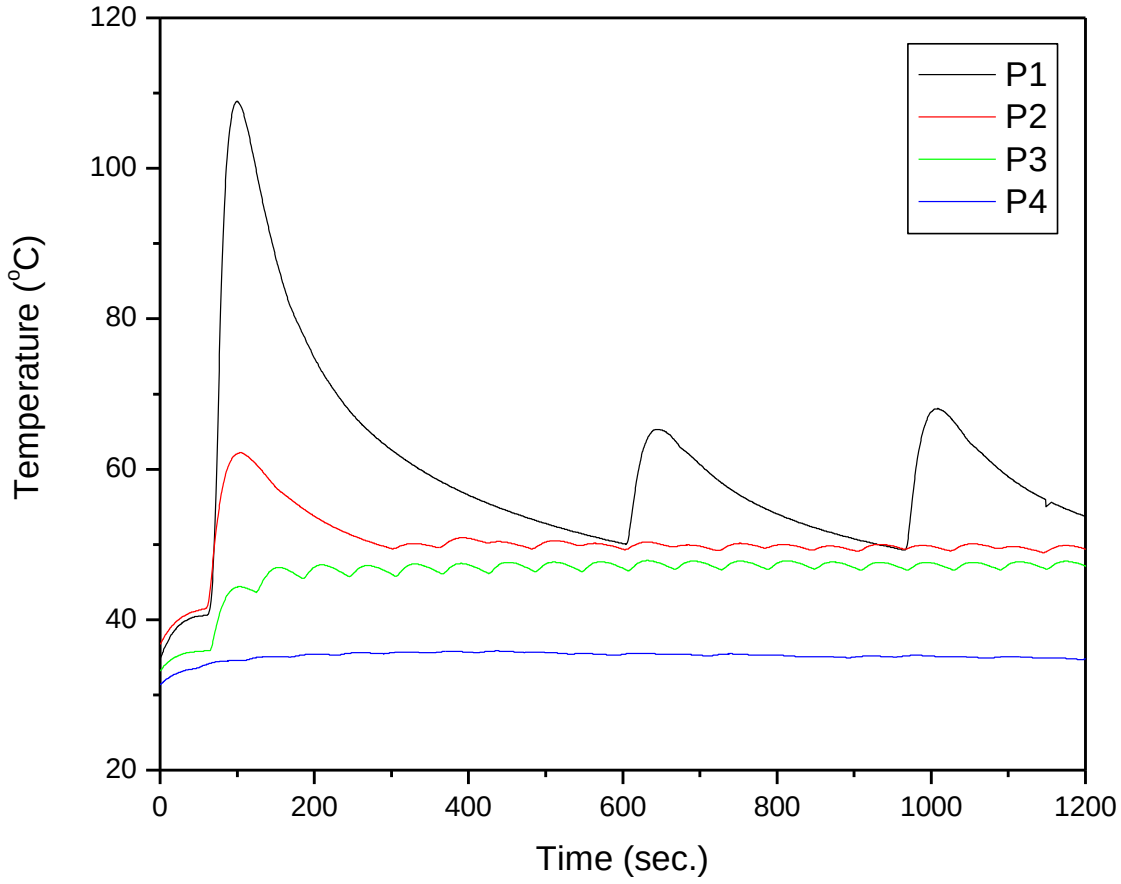

Figure 5.1: Temperature – time graph for P-systems at 50°C set point

It was observed that the increase in proportional value lowers the overshoot at the transient phase. The increase in proportional value also contributes to the stability of the system's response. This is clearly observed in set P2 where a better steady state condition is seen in comparison to set P1. It is set P2 that recovers faster than set P1 from the overshoot to stability. This is observed through the peak amplitude of their overshoot. However, set P1 steady state conditions are not desirable as for its great steady state range when compared to that of set P2 and P4. Finally, even though set P4 has a stable steady state, the error is too big and the system never reaches the desired set point. It was observed when the proportional value is high, the system yields a low transient response. Furthermore, an extremely lower proportional value yield unstable steady state conditions and extremely high proportional value yield system that never reach set point. High proportional value

bring stable state with errors while low value shows unstable system's response (see P4 in Figure 5.1). Various other behaviour yield by proportional control tuning is presented on Figure B1, B2 and B3 on Appendix B.

5.2 PROPORTIONAL INTEGRAL SYSTEM

This system is looking at investigating the impact of varying while leaving derivative value at zero. This type of system is a common system that is perceived as an improvement of the proportional system and sometimes challenging to control. According to the literature reviewed in Chapter two, tuning or adjusting the integral parameter tends to reduce or increase the steady state offset better known as error. The impact of the integral is better demonstrated when comparing its impact before considering the proportional system. Therefore, the sets in this section presents the impact of the PI systems. Three varying integral values were tuned for the same proportional value. This was repeated for three proportional values 10, 40 and 500 subsequently which were properly tested in the proportional system. The system behaviours were observed as tabulated and then graphically presented.

Table 5.2: PI-system parameters 1

	Parameter		
Set	**P**	**I**	**D**
PI 1	10	10	0
PI 2	10	100	0
PI 3	10	1000	0

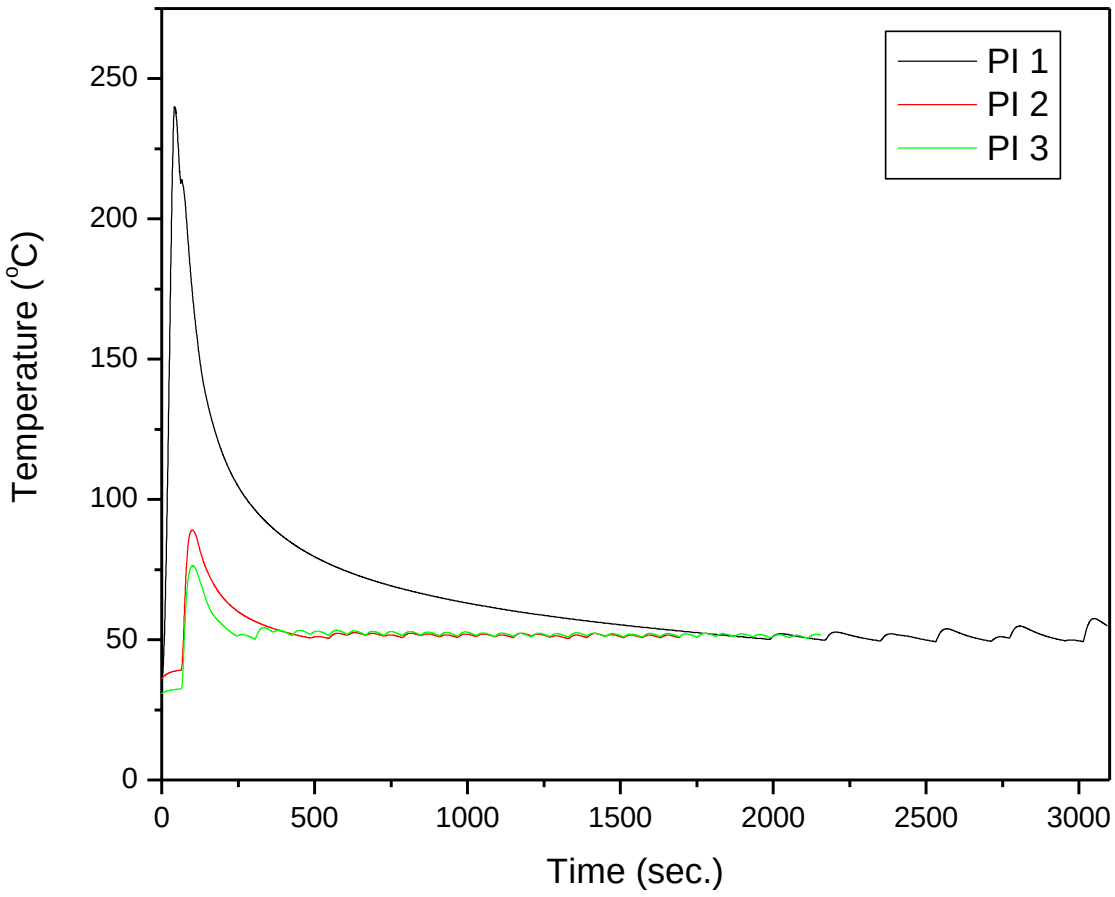

Figure 5.2: Temperature – time graph for PI-system 1 at 50°C set point

Table 5.3: PI-system parameters 2

Set	Parameter		
	P	I	D
PI 4	40	10	0
PI 5	40	100	0
PI 6	40	2000	0

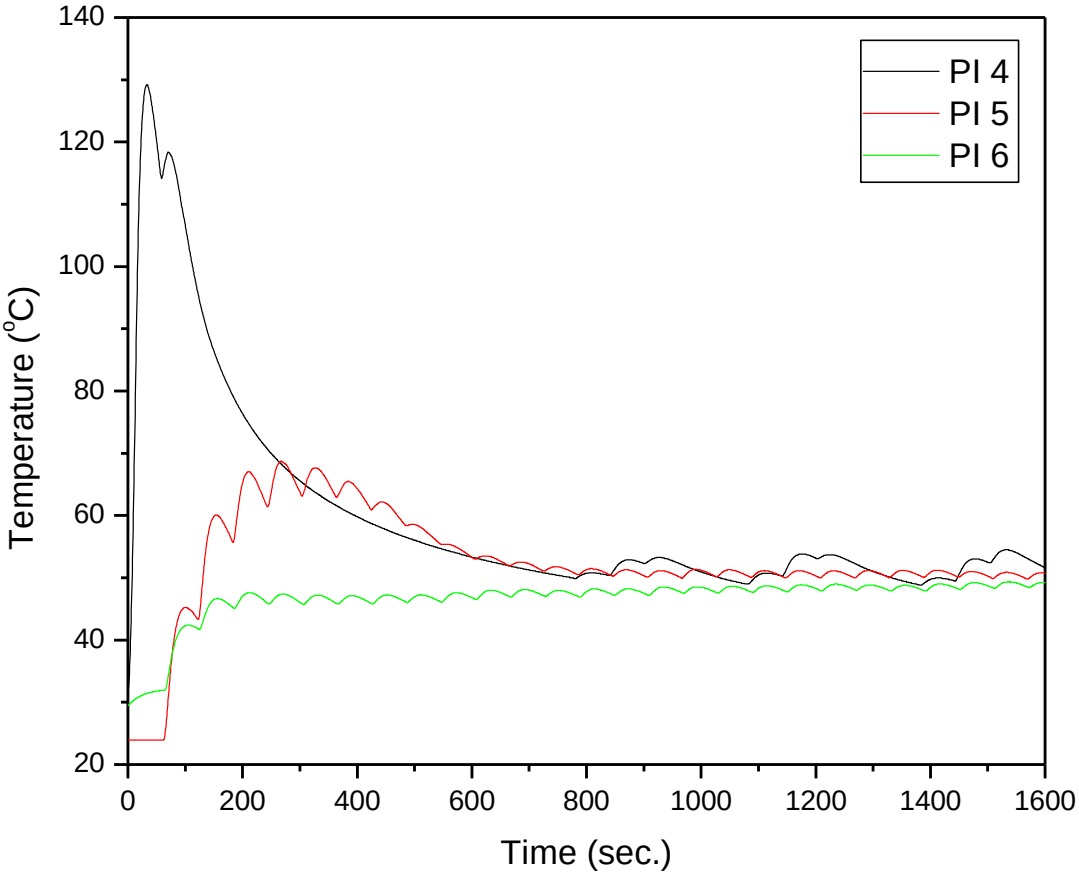

Figure 5.3: Temperature – time graph for PI-system 2 at 50°C set point

Table 5.4: PI-system parameters 3

Set	Parameter		
	P	I	D
PI 7	500	10	0
PI 8	500	100	0
PI 9	500	1000	0

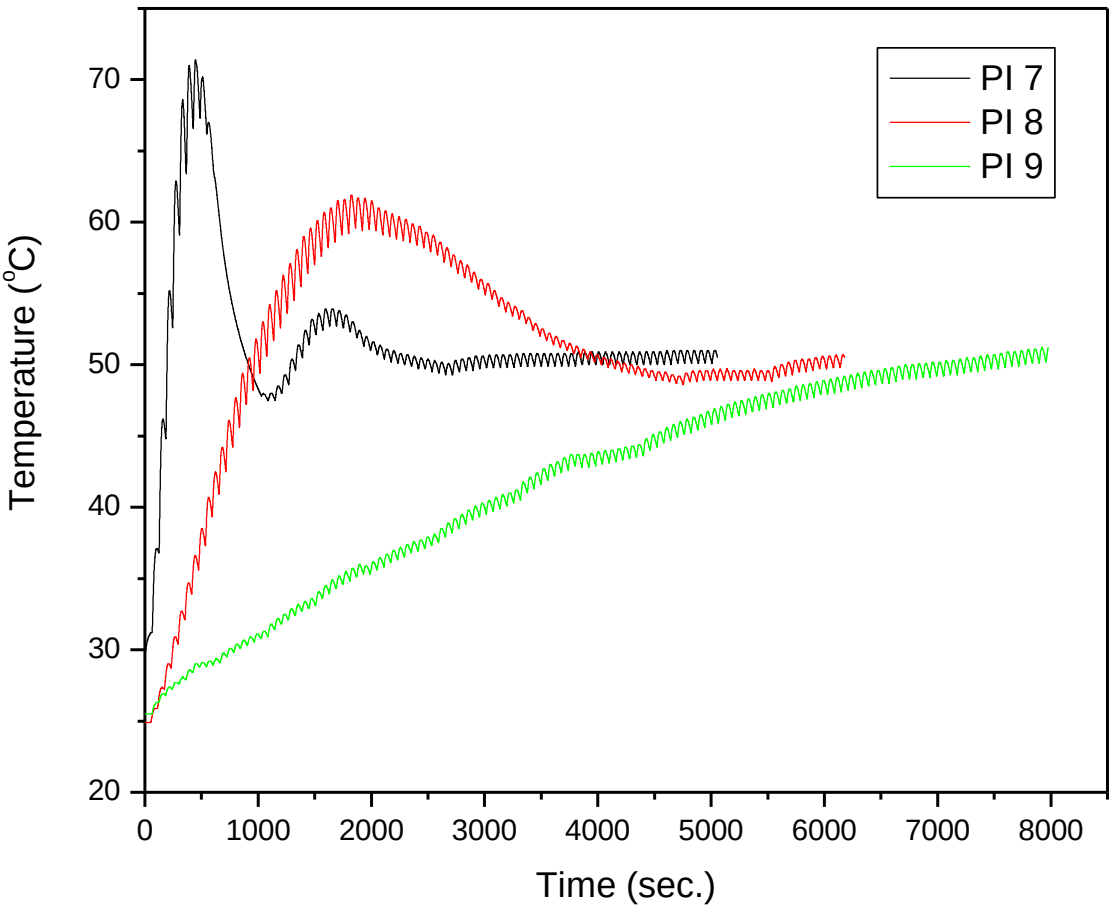

Figure 5.4: Temperature – time graph for PI-system 3 at 50°C set point

Now, with the prior knowledge from the literature reviewed the proportional integral (PI) systems are an improvement of the proportional systems that have adjusted steady state error with an aid of tuning the integral value. The tests performed in the previous section 5.1 were only proportional, the integral was then introduced to the sets in this section of the proportional integral system. It was observed that introducing the integral parameter to the proportional system had an impact on the transient phase. This was evident when one compares set P1 on Figure 5.1 and all sets on Figure B4 on Appendix B. What was observed was that, when an extremely low proportional and integral value was tuned, this amplified the overshoot in the transient phase and exhibits unstable steady state conditions. For proportional integral systems with proportional values of 10 and higher, as seen on Table 5.3 and 5.4 showed that as the integral value were increased the systems transient phase changed. The overshoot gradually decreased which decreased the aggressiveness of the system, this caused it to eventually be moderate at the highest integral value of the same proportional value.

When the proportional integral systems tests were performed it was observed that, the PI 3 set was the one to reach steady state at 244 seconds which was more in the direction of what is desired to be achieved out of the experiments. This set also exhibited the lowest amplitude of the overshoots on the

figure. Furthermore, another shape of graph noticed was on set PI 9 which reached steady state after 8000 seconds. This sort of behaviour is too slow (moderate) causing the system to take long to reach steady state conditions which is not desired in this study. However, the integral parameter was later further explored in the three term system which is also known as the PID system.

5.3 PROPORTIONAL DERIVATIVE SYSTEM

This system is looking at investigating the impact of PD values. The proportional parameters were set to be 10, 40 and 500 and then the derivative parameters were set in an ascending order of 10 to 425 and then 950 on the controller for all three sets. The performance of these systems were compared to that of proportional systems observed in Figure 5.1 to see the impact of the derivative on the proportional system.

Table 5.5: PD-system parameters 1

Set	Parameter		
	P	I	D
PD 1	10	0	10
PD 2	10	0	425
PD 3	10	0	950

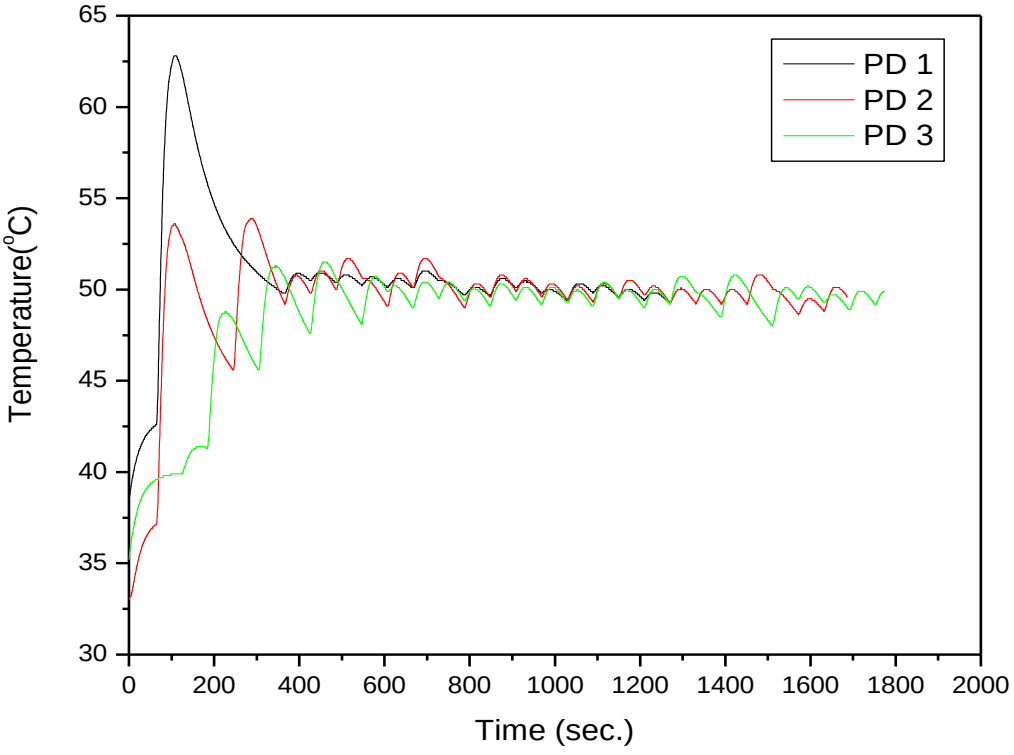

Figure 5.5: Temperature – time graph for PD-system 1 at 50°C set point

Table 5.6: PD-system parameters 2

Set	Parameter		
	P	I	D
PD 4	40	0	10
PD 5	40	0	425
PD 6	40	0	950

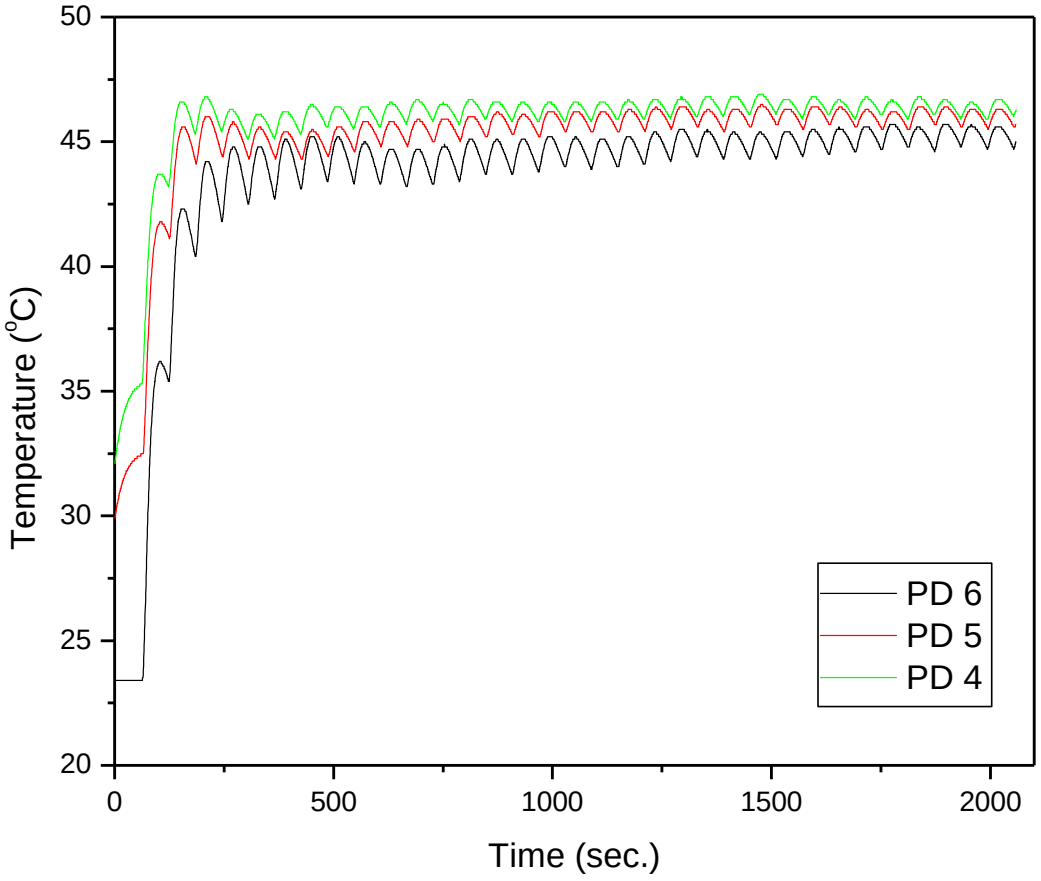

Figure 5.6: Temperature – time graph for PD-system 2 at 50°C set point

Table 5.7: PD-system parameters 3

Set	Parameter		
	P	I	D
PD 7	500	0	10
PD 8	500	0	425
PD 9	500	0	950

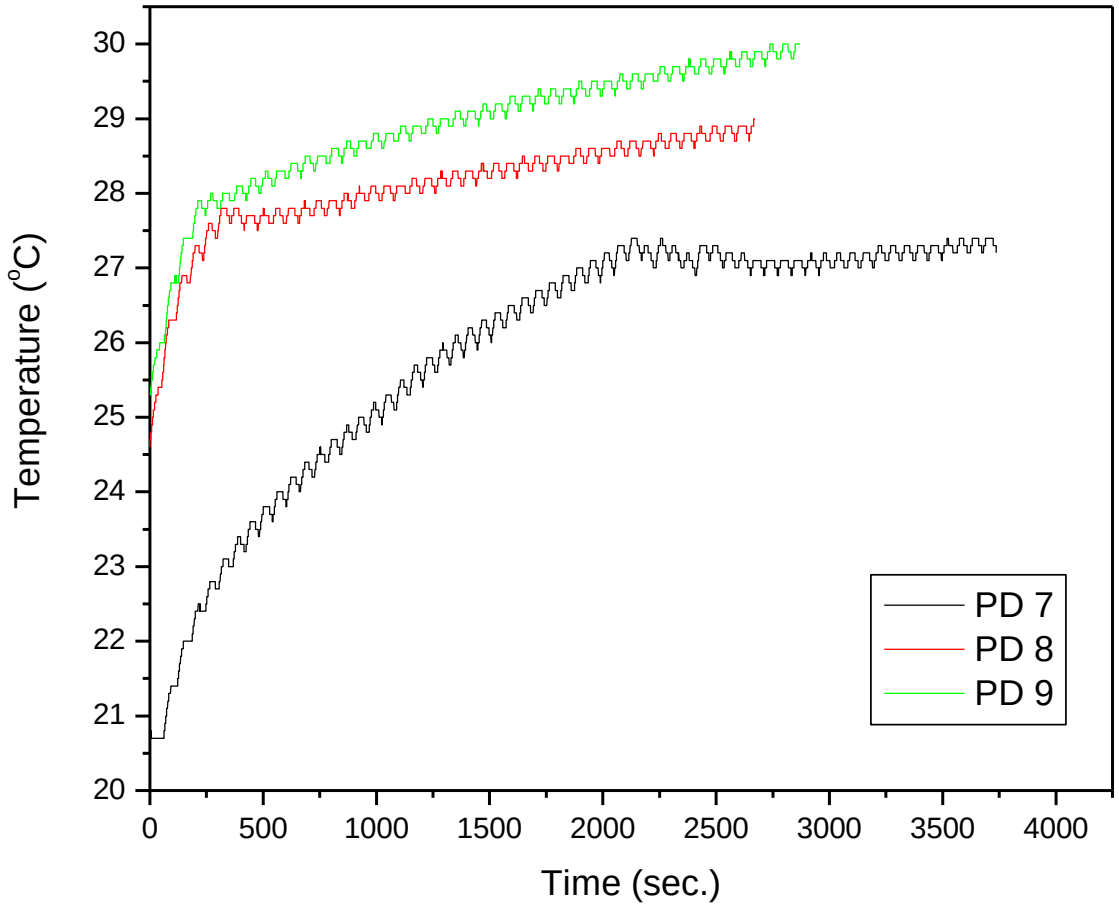

Figure 5.7: Temperature – time graph for PD-system 3 at 50°C set point

It was observed that in the proportional derivative systems which has low proportional value of 1 as seen on Table B5 on Appendix B yields an unstable system regardless of the set derivative. It was further observed that the sets with the proportional values tuned below 10 yield a system with an overshoot. However, those systems that had a proportional value tuned to 10 and above such as the ones on Figure 5.6 and 5.7 yield systems that had no overshoot. This was due to the high proportional value of the systems. The proportional derivative system exhibited a consistent behaviour whereas the derivative value was increased, the transient phase was affected by a gradually lowered overshoot.

5.4 PROPORTIONAL INTEGRAL DERIVATIVE SYSTEMS

After the impact of adjusting the P, I and the D values on the reviewed system had been distinguished, two sort of behaviours were common in all the test results which were graphically analysed on the temperature- time profiles. These profiles were demonstrated in the P, PI, PD and now the PID systems which are presented in this section and onwards. The first shape was the one with a high over shoot

in the transient phase as set PID 1 and 2 showed below. The second shape was the one without an overshoot at transient phase seen on set PID 3 and 4. These two type of graphs validate the reviewed literature on moderate and aggressive tuning that was presented in Chapter 2. Table 5.8 shows moderate and aggressive random tuning. Set PID 1 and 2 were aggressive tuning yielding a fast responding system and set PID 3 and 4 were moderate tuning yielding a slow responding system.

Table 5.8: PID-system parameters

Set	Parameter		
	P	I	D
PID 1	10	20	30
PID 2	80	20	30
PID 3	190	500	500
PID 4	210	500	500

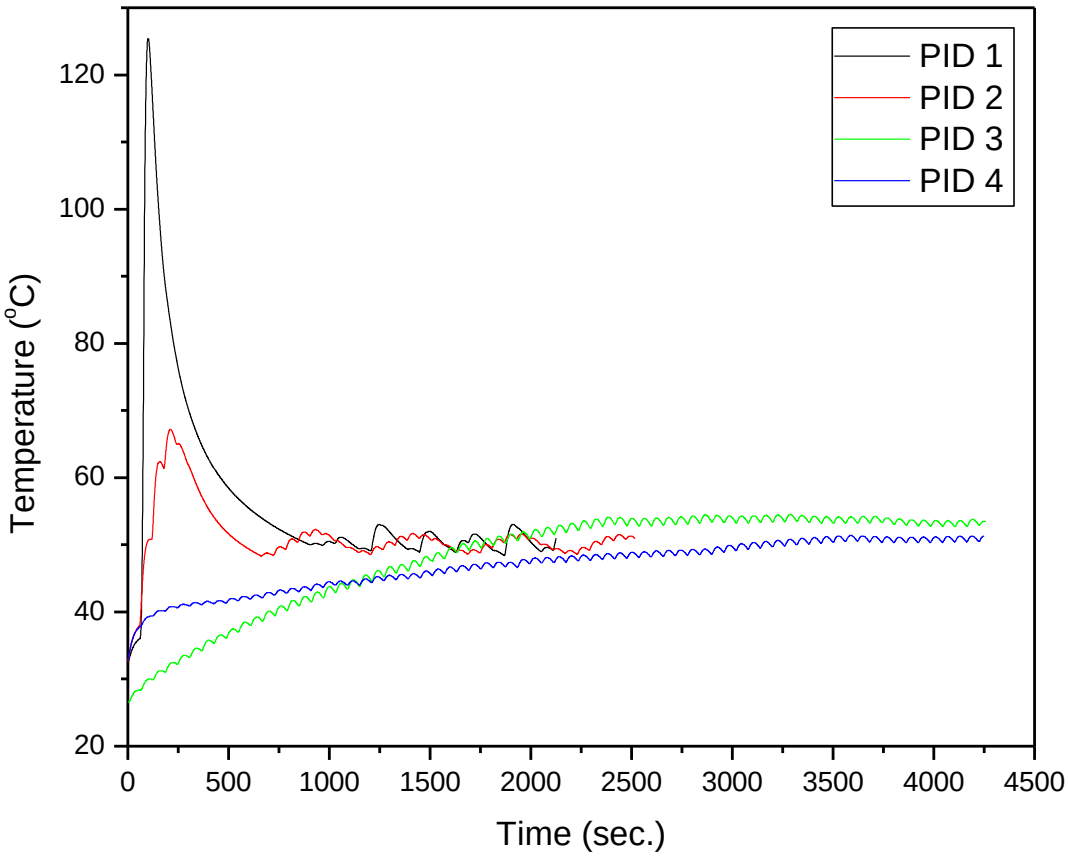

Figure 5.8: Temperature – time graph for PID systems at 50°C set point

Now that the parameters of P, I and D had been individually investigated, for the impact that they have on the behaviour of the system, the combination of all three parameters were then tested. In those tests performed, the shortest time that the system could reach steady state condition was targeted as

per objective f) in Chapter 1. The literature reviewed verified that aggressive tuning yields a desirable temperature-time profile shape which was observed in most tests. The graphs on Figure 5.8 distinguishes that set PID 3 and 4 takes long to reach steady state condition when compared with the graphs of set PID 1 and 2. It should be noted again that all tests were performed at the set point which was 50^{o}C.

The overshoot is not a problem, due to the type of material that was initially the benchmark specimen to be tested which is the shape memory alloy specimen. This material can withstand extremely high temperatures as reviewed on the literature in Chapter two. This was used as an educative guideline to approximate of the acceptable percentage overshoot of the system. The acceptable percentage overshoot which is measured from the set point temperature and, the duration of the overshoot should be kept short so that it does not interfere with the microstructure of the shape memory alloy. This was confirmed by Case et al., (2004) study where they demonstrated that exposing SMA to a temperature of above 500^{o}C for 10 minutes or more will interfere with its microstructure. Based on this information the overshoot should recover in less than 10 minutes. This condition disqualifies PID 1 since its recovery period exceeds 10 minutes. PID 2 becomes the best option since it recovery period is less than 10 minutes. The microstructure of the specimen to be tested will not be disturbed when tested, due to the temperature range that the chamber is intended to perform tests at. Therefore, the tests performed further from this point were developed based on the parameters and shape of the graph of set PID 1 and 2 because of its ability of reach steady state faster. Even though set 1 has high peak overshoot it was still further tested with adjusted values to reduce its amplitude and duration time of the overshoot. The reduction of the percentage overshoot was to be less than 35% of the set point in the transient phase so that the recovery time from the overshoot is shorten and reaches steady state in less than 10 minutes.

5.4.1 PID systems of varying proportional values

To this point it has been experimentally demonstrated that aggressive tuning consists of a low integral and derivative values and vice versa for moderate tuning. This is evident on Table B4 and B5 on Appendix B. On the other hand, the proportional value single handily exhibits aggressive tuning when its value is kept lower. The impact of the proportional value was further investigated on a PID system. Three set of parameters of I=20 and D= 30 were set, only adjusts the P value from 10 to 40 and then 160. As discussed previously on the proportional system, that adjusting the P value affects the transient phase. This was also witnessed in this system which had the addition of the integral and the derivative values.

Table 5.9: PID parameters of varying P values

Set	Parameter		
	P	I	D
PID 5	10	20	30
PID 6	40	20	30
PID 7	160	20	30

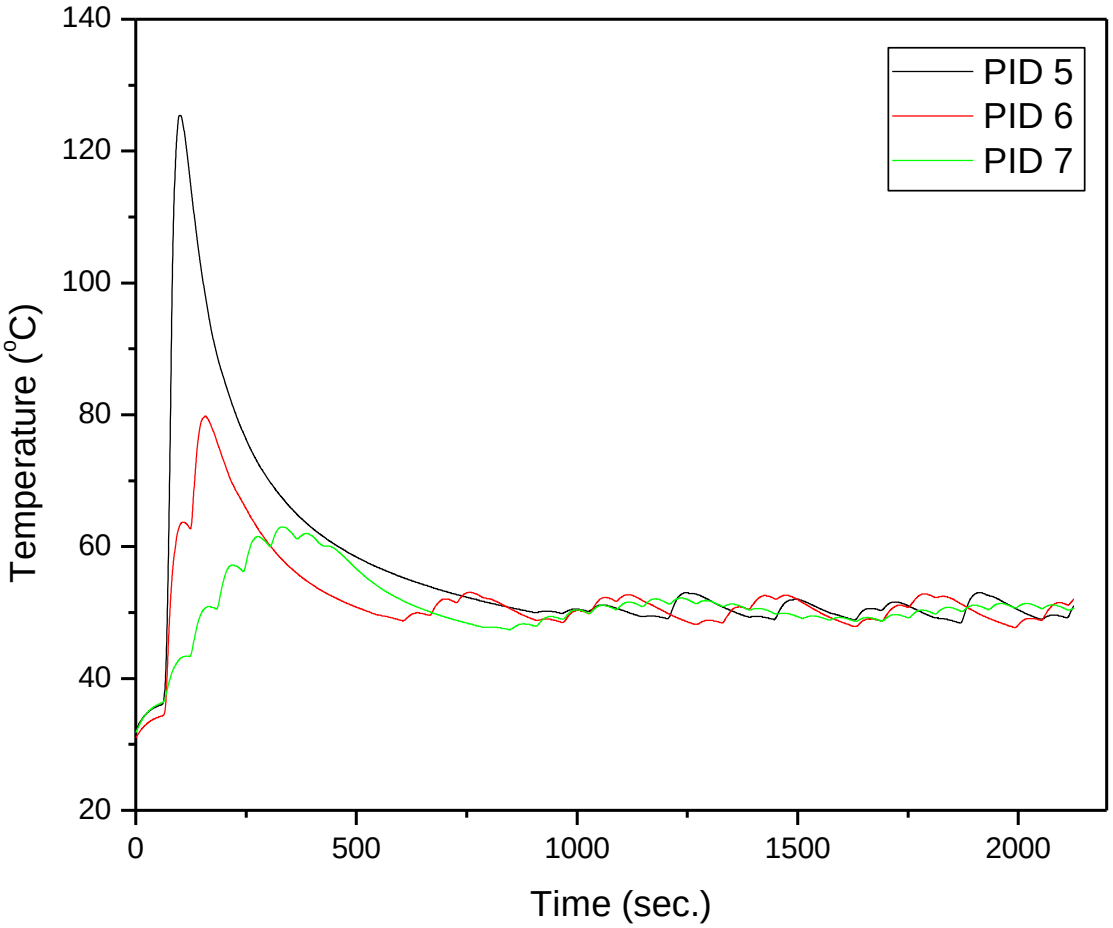

Figure 5.9: Temperature – time graph for varying P-value PID systems at 50°C set point

In the transient phase it was observed that a higher proportional value yields less overshooting in the system. A lower overshoot resulted in the steady state being reached earlier, this is evident from the graph in Figure 5.9 if set PID 6 and 5 are compared. However, set 7 does not reach steady state faster than set PID 5. This is caused by less peak sharpness overshoot for and the moderate tuning of the proportional value of this set. Therefore, it was evident that varying the proportional value in a PID system does not only affect the transient phase but also the steady state condition. This was observed when the three sets presented on Figure 5.9 demonstrated various behaviours. Set PID 7 had the most stable steady state in comparison to the other two sets on the Figure 5.9

Set PID 5 has the same proportional value with set P2 but the overshoot in set PID5 doubles that of P2 in Figure 5.1. When comparing set PID6 with P3 on Figure 5.1 we see an overshoot on set PID 6 which was not seen on set P3. Also compare set PID7 and P160 on Figure B2 Appendix B, PID 7 has an overshoot whereas P16 stabilized at 38^{o}C. All these systems have similar behaviour, it was concluded that the presence of the integral and the derivative had caused the system to have an overshoot which is higher than the initial proportional systems.

5.4.2 PID systems of varying integral values

Experiments were performed to further investigate the impact of the integral value which was then tested in the PID system. The integral value was varied from 0 to 50 and then 100, the derivative values were tuned to 100 and these were kept constant for 40 and 80 proportional values. These two values were selected based on the outcomes of set PID 6 on Figure 5.9 where it was concluded that the steady state is reached the fastest in those combination, but it was not clear as to how does the integral the derivative affected the behaviour of the system. Therefore, Table 5.10 and 5.11 addressed that concern on the integral perspective.

Table 5.10: PID parameters 1 of varying I values

Set	Parameter		
	P	I	D
PID 8	40	0	100
PID 9	40	50	100
PID 10	40	100	100

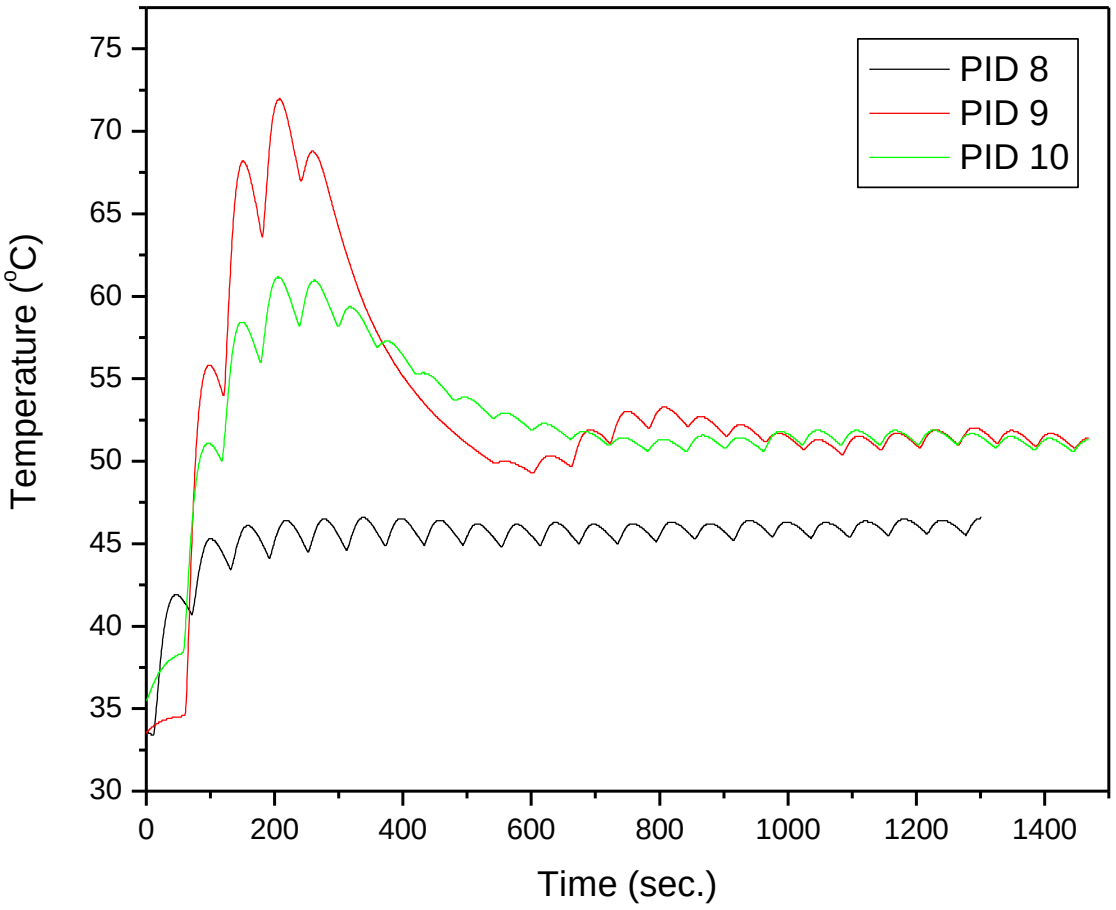

Figure 5.10: Temperature – time graph for varying I values of PID system 1 at 50°C set point

Table 5.11: PID 3 parameters 2 of varying I values

Set	Parameter		
	P	I	D
PID 11	80	0	40
PID 12	80	50	40
PID 13	80	100	40

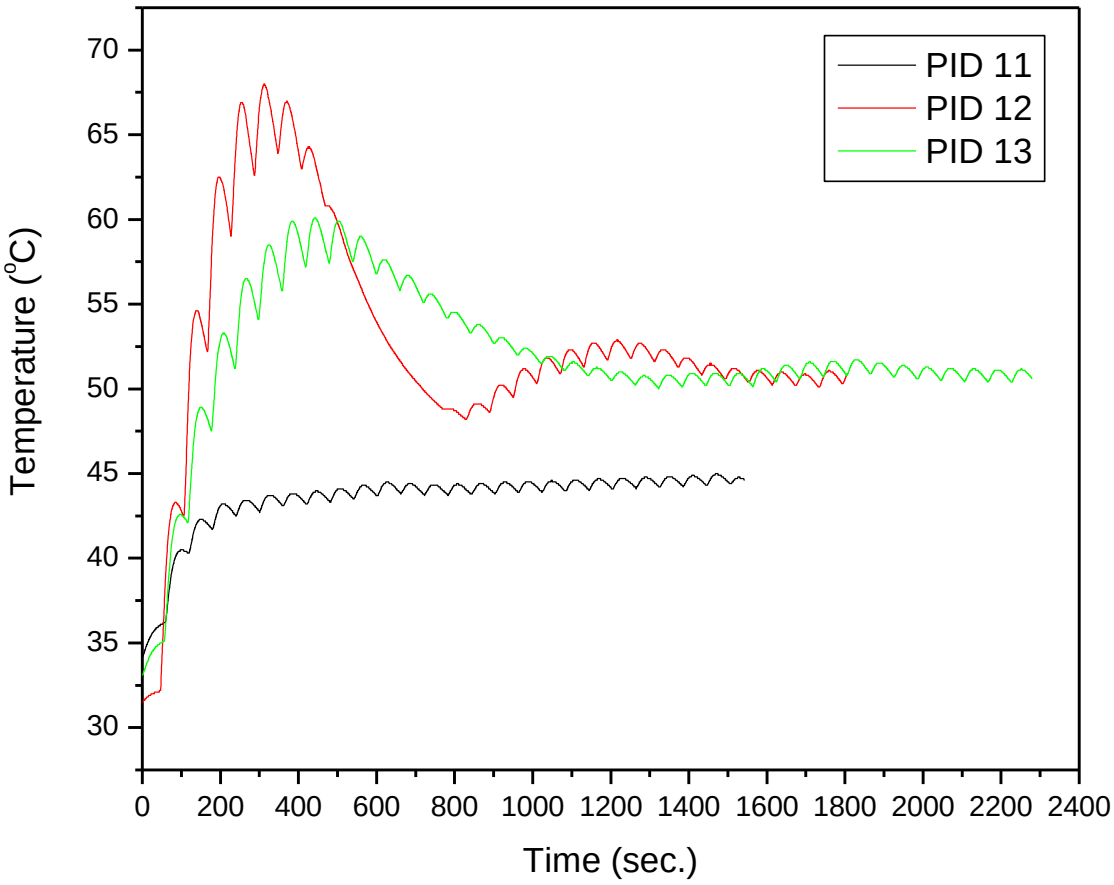

Figure 5.11: Temperature – time graph for varying I values of PID system 2 at 50°C set point

It was discovered that the system goes from moderate to aggressive upon gradual increase in integral value. This was also observed on the sets on Figure 5.11. These behaviours verify what were experimented in section 5.2. The integral value impacted the steady state error and the transient phase. This was observed when the amplitude of the overshoot varied even though the proportional value was kept constant. The reason for this was, to attempt to reduce the steady state error which was seen on set PID 11. The steady state errors were due to the parameters which yielded an undesirable system response. The increase in integral value indirectly affected the transient phase. The system ended up reaching the set point. However, the overshoot was one of the dynamics that needed to be adjusted in the investigation.

5.4.3 PID systems of varying derivative values

This section is looking at the investigation of the impact of varying derivative values while keeping other parameters constant. The P and I values were kept between 10 and 500 while varying the D values from 10 to 800 (see Table 5.12-13).

Table 5.12: PID 3 parameters 1 of varying D values

Set	Parameter		
	P	I	D
PID 14	10	10	10
PID 15	10	100	100
PID 16	10	1000	800

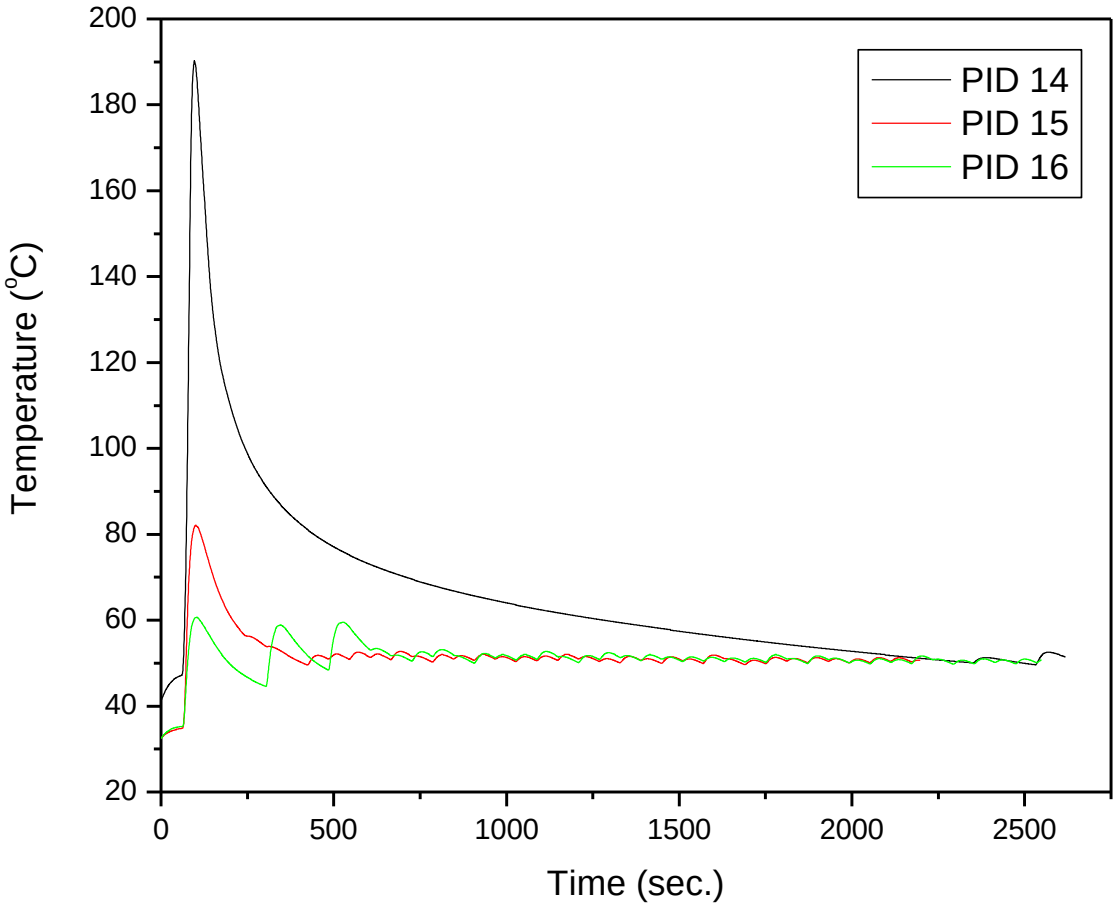

Figure 5.12: Temperature – time graph for varying D values of PID system 1 at 50°C set point

Table 5.13: PID 3 parameters 2 of varying D values

Set	Parameter		
	P	I	D
PID 17	500	10	10
PID 18	500	10	100
PID 19	500	10	800

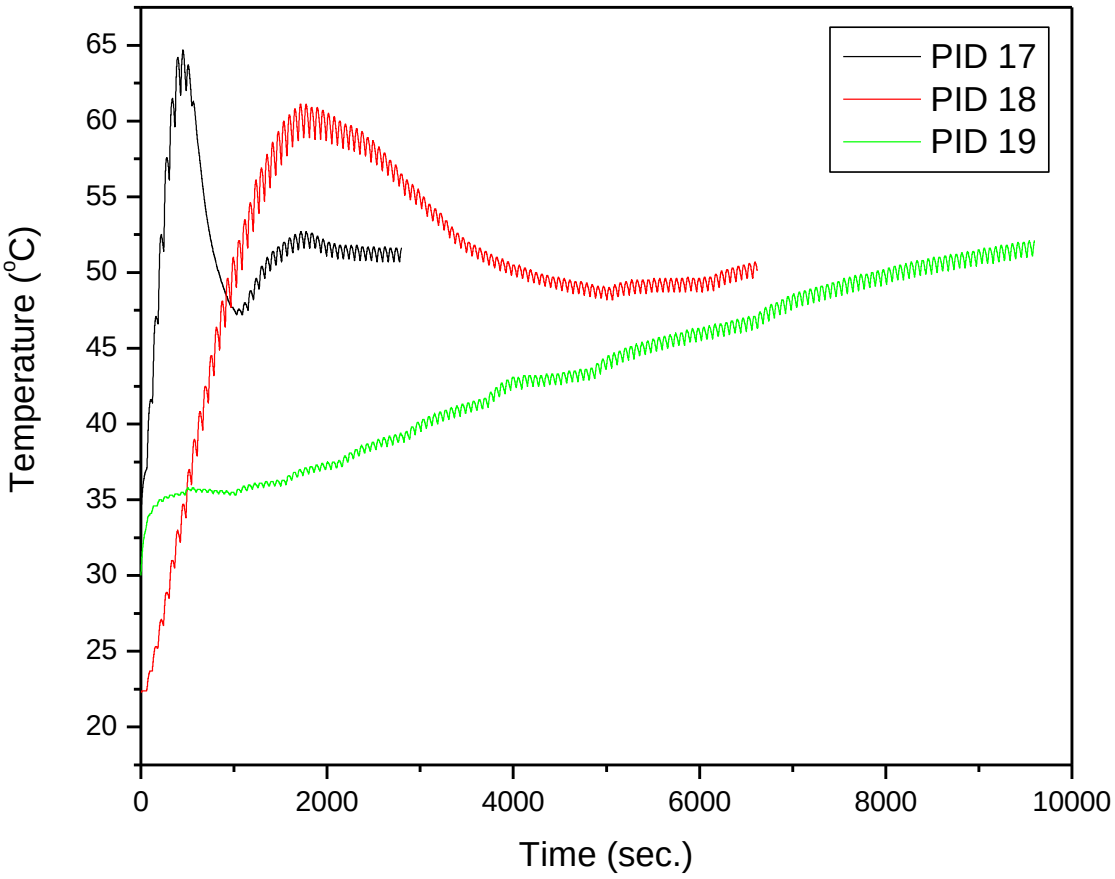

Figure 5.13: Temperature – time graph for varying D values of PID system 2 at 50°C set point

Initially, the proportional value created the overshoot in the system. After running several tests, it was observed that the derivative value also impacts the transient phase resulting in the overshoot which was seen in the PID system. This behaviour was distinctly confirmed again in Figure 5.13 presented systems behaviour where, when the derivative was increased for the same set of proportional values the amplitude of the overshoot decreased. However, these behaviours were compared to set P2 on Figure 5.1 where the overshoot of proportional system having a value of 10 overshoot reached 63°C. It was noticed that even though the overshoot decreases with the increasing derivative value on Figure 5.13 these overshoot were higher than that of set P2. This was also observed when comparing set P3 on Figure 5.1 with systems presented on Figure 5.14 behaviours. This sort of behaviour of amplified overshooting however causes the steady state conditions to be delayed especially for low derivative values that were observed on the PID 19 set on Figure 5.13. The cause of this is the presence of the other two parameters which individually contribute to the overshoot. These systems were compared with those on Figure 5.1 because of the same proportional value they had.

5.6 COMPARATIVE DISCUSSION AND SUMMARY

Based on the experiments that were performed, the impact of parameter variation was analysed with an aid of the range band presented on Figure 5.14. This was done for all three parameters to demonstrate their impact on the system.

This was formulated with reference to the information provided by the catalogue which indicates the maximum of 999.9 and minimum of zero for the proportional values of the controller and the accumulated results from the experiments. It was observed that a high proportional value resulted in a slow and moderate system which is on the far right end of the band. It was also evident that at this end the system yielded a large steady state error and no overshoot as seen in set P3 of Figure 5.1. On the contrary an aggressive system was exhibited when the tuning had low proportional values.

Figure 5.14: Proportional tuning effect

The same was done to illustrate the effect of tuning the integral values. The minimum and maximum values for the integral time are (0 and 3600) respectively as indicated by the controller manufacturer's manual. The tuning of this parameter was done at the presence of the effect of proportional value. All systems have the proportional component in any type of tuning, hence it is said that both improve the proportional system. The integral had an effect on the steady state error and this was confirmed experimentally. Although literature and the tests results proved that the proportional integral system improves the stead state conditions, it was also found that it does have an effect on the transient phase and this was evident on Figure 5.3. However, in the presence of low proportional value the integral did not have much visible effect on the transient phase. This was evident on Figure B4 on the Appendix B. Therefore, the proportional value had to be 10 and above for the integral to affect the transient phase. It was also evident that the below Figure 5.15 is highly relevant to a proportional integral system. The proportional value that is above 10 and an integral value that is high as seen on Figure 5.4 yields a slow system.

Figure 5.15: Integral tuning effect

The derivative has a maximum of 999.9 value indicated by the manufacturers controller manual. It was observed that a low derivative value yields a highly aggressive overshoot at the transient phase more especially a combination of a low proportional value below 10. Slow or moderate systems were observed in systems where high derivative values were tuned. This parameter did not alter the steady state condition but rather it just delayed or accelerated it, based on the transient phase response whether it is aggressive or moderate.

Figure 5.16: Derivative tuning effect

It was confirmed that a three term controller had better control over the system even though it is complex to control. Each parameter had its individual impact on both transient and steady state phases whether directly or indirectly. However, with the accumulated understanding on how these parameters affect or contribute to the system's behaviour, one was able to select the optimal parameters for the system. Table 5.14 shows the optimal combination values of the PID system to control the heating process of the chamber.

Table 5.14: Final PID parameters

Set	Parameter		
	P	I	D
Optimal 1	10	100	150
Optimal 2	10	100	120
Optimal 3	10	100	135

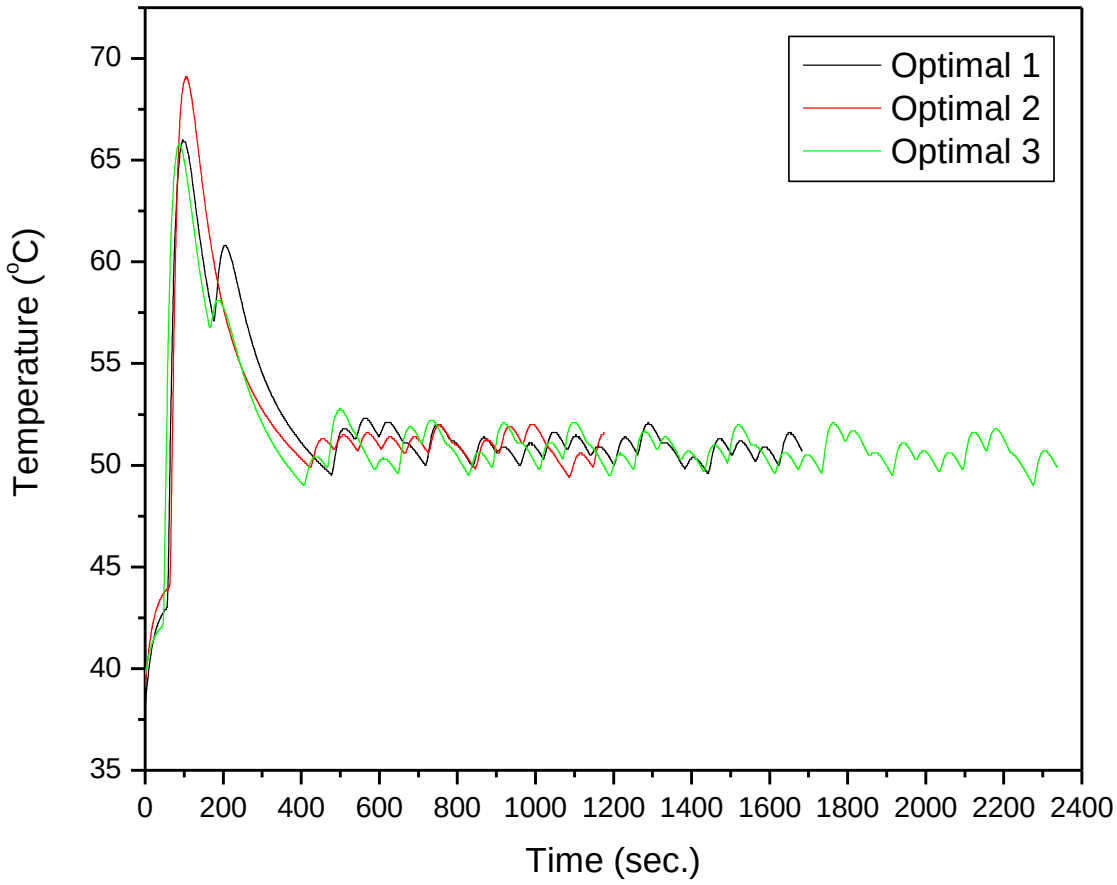

Figure 5.17: Temperature – time graph of three optimal tuning system behaviour at 50°C set point

Table 5.15: Final results analysis

Set	Overshoot peak (°C)	Overshoot peak (%)	Overshoot recovery time (sec.)
Optimal 1	65.9	31.8	490
Optimal 2	69.1	38.2	440
Optimal 3	65.8	31.6	400

$$\% \text{ os} = \left[\left(\frac{\text{os} - \text{sp}}{\text{sp}} - 1\right) \times 100\right] \quad (16)$$

Table 5.15 shows the temperature peak of the overshoot (os) and the percentage of the overshoot measured from the set point is presented. The percentage overshoot was calculated using equation (16). From these calculations, set Optimal 3 had the least percentage overshoot. However, it is also evident from Figure 5.17 that set Optimal 3 recovers the overshoot faster than the other two sets. Hence, this set was the finally tuned combination that the chamber operate in. It was stated in section 5.4 that the desired percentage overshoot is to not exceed 35% of the set point temperature. This was successfully achieved with 31.6% overshoot which is within the range stipulated initially. Also, the overshoot duration time was 400 seconds which was the shortest of all and less than 10 minutes.

5.7 CHAMBER'S MAXIMUM TEMPERATURE TEST RESULTS AND DISCUSSION

After the shell of the chamber had been manufactured and powder coated test were also necessary at this stage. In this test the final outside temperature was investigated using the infrared thermometer at set temperature 350^{o}C, which is the maximum temperature that the chamber is designed for. Table 5.16 presents the different parameters that were tuned and the temperature that the infrared thermometer recorded on the outside shell of the chamber.

Table 5.16: Outside temperature results of the shell at set temperature 350^{o}C

Set Parameters	P	I	D	Overshoot peak (^{o}C)	Outside temp. (^{o}C)
Optimal 3	10	100	135	485	47
PID 30	250	20	5	450	36
PID 31	650	10	100	430	34

Due to the *Explorer GLX* data logger having a plastic cover on its thermocouple, these tests data could not be logged because of the extremely high temperature that was in the chamber and therefore the overshoot peak was virtually recorded. However, the purpose of this test was to confirm the outside temperature of the chamber. With the previously observations that showed that a high proportional value exhibits a low overshoot, this was used to determine the ideal parameters of the chamber when it is operating at 350^{o}C. The optimal combination values were further optimised with the purpose of reducing the shell temperature. Therefore, set combination PID 31 was concluded to be the optimal combination when the personnel is operating the chamber between 250 and 350^{o}C. The percentage overshoot of this set was 22.9%. Therefore, it can be concluded that as the set point or temperature is increase the percentage overshoot should be decreased to hedge against high external temperature of the shell.

Even though the controlled tensile test results are not part of the conducted study, these tests were necessary for demonstration purposes. When these tests were performed first a length of 75mm was tested at room temperature. The tensile tests were performed at the various indicated temperatures. See results on Appendix C

There was a still a challenge of not achieving the close loop stress-strain graph due to faulty tensile testing machine extensometer. However, should the extensometer available had been working the desired graph of the behaviour of the SMA wire at controlled temperature would have been achieved.

CHAPTER 6
CONCLUSION AND RECOMMENDATIONS

6.1 CONCLUSION

The chamber was successfully manufactured and tested at the maximum operating temperature (350^{o}C). However, it was established that different combinations were tuned for various temperature ranges to prevent the chamber to overheat on the outside. This was due to the nature of the shape of the desired graph that depicts the system response. The desired graph shape for this study was that of a fast response system which meant an overshoot was acceptable. However, an increase in set point temperature resulted in an unsteady system response. Therefore, the parameters had to be re-tuned for the temperature ranges close to maximum operating temperature. Initially the acceptable percentage overshoot was 31.6%. After the further tests had been performed at maximum temperature the initially concluded parameters which were performed at 50^{o}C had to be adjusted for the maximum temperature test. Therefore, new parameters were tuned for the maximum operating parameters. These new parameters had to impact the system by reducing the percentage overshoot at set point 350^{o}C so that the shell temperature of the chamber is not too hot.

It can be concluded that aggressive tuning was ideal for this system. This was per objectives of study which indicated that the system should reach steady state at the shortest possible time. The tests that were conducted in order to determine the working combination were successful. Even though there were data logging constraints for higher temperature ranges, all tests were performed at 50^{o}C. The shell temperature for the chamber at maximum test temperature was recorded using the infrared thermometer.

6.2 RECOMMENDATIONS

For future work, it appears that there is still room for improvement for the design of the chamber. The following can be done to improve the chamber designed and manufactured in this study:

a. The back of the chamber
b. Detachable handles to carry the chamber
c. Specimen connector design

A special cover for the back of the chamber that is made out of special temperature resistant material is recommended for future improvement design. This will increase the safety of the machine.

Detachable handles to carry the chamber are recommendable. This will allow easy mobility of the chamber and protecting the chamber from being mishandled at sensitive parts such as the control box and the back of the chamber.

The specimen connector design has a lot of room for improvement. More especially the top connector can be improved to eliminate the obstruction of the clamping bolt and nuts which will allow a greater maximum specimen length to be tested. The shape of the specimen connector can be altered. Finally, the material selection can be improved as for the on currently designed was manufactured out of mild steel.

BIBLIOGRAPHY

Akiyoshi, M.M., Christoforo, A. L., Luz, A. P. & Pandolfelli, V. C. 2017. Thermal conductivity modelling based on physical and chemical properties of refractories. *Ceramics International.* 43:4731-4745

Bockris, J. O., White J. & Motzfeldt, K. Ed. 1959. *Physicochemical Measurements at High-Temperatures.* London: Butterworths.
Available: https://archive.org/stream/physicochemicalm00bock#page/n6/mode/1up

Case, L. Kreiner, Z. Redmond, J. Trease, B., 2004. *Shape Memory Alloy Shape Training Tutorial*. (A teacher's guide to teaching SMA training).

Cengel, Y.A. & Boles, M.A. 2008. *Thermodynamics.* 7th ed. New York: McGraw Hill.

Control Guru. n.d. *Heat Exchanger PI Control Test*. Available: http://controlguru.com/pi-control-of-the-heat-exchanger/

Davis, J.R. 2004. *Tensile Testing.* 2nd ed. United States of America: ASM International.

Dolezal, R. 1967. *Large Boiler Furnaces*. New York: Elsevier Publishing Company.

Energy Managers and Energy Auditors. n.d. *Insulation and Refractories*. Available: http://www.em-ea.org/guide%20books/book-2/2.5%20insulation%20&%20refractories%20.pdf. [August 2016].

Gan, J., Zhang, X., Li, H. & Wu, H. 2017. Full Closed-loop Controls of micro/nano positioning system with Nonlinear Hysteresis using micro-vision system. *Sensors and Actuators.* 257:125-133.

Ghobara, Y.E.M. 2013. *Modeling, Optimazation and Estimation in Electric Arc Furnace (EAF) Operation.* Master of Applied Science Thesis. McMaster University.

Halvorsen, S.A., Olsen, H.A.H. & Fromreide, M. 2016. An Efficient Simulation Method for Current and Power distribution in 3-Phase Electrical Smelting Furnaces. *IFAC-Papers OnLine*. 49(20):167–172.

Han, P. 1992. *Tensile Testing*. United States of America: ASM International.

Han, Y., Geng, Z., Wang, Z. & Mu, P. 2016. Performance analysis and optimaltemperature selection of ethylene intergrated analytic heirarchy process. *Analytical and Applied Pyrolysis*. 122:35–44.

Hannon, A. & Tiernan, P. 2008. A review of planar biaxial tensile test system for sheet metal. *Materials processing technology*. 198:1–13.

Harbison Walker. 2017. *Handbook of Refractory for Incineration Systems*. Available: http://www.banksengineering.com/Refrac%20Properties%20-%20definitions.pdf

Holman, J.P. 2010. Heat Transfer. 10thed. United State of America: McGraw-Hill.

Janna, W.S. 2011. *Design of Fluid Thermal Systems.* 3rd ed. United States of America: Global Engineering.

Jiang, H., Xu, X., Omori, T., Nagasako, M., Ruan, J., Yang, S., Wang, C., Lui, X. et. al. 2016. Martensitic transformation and shape memory effect at high temperatures in off-stoichiometric CO_2VSi Heusler alloys. *Material Science & Engineering A*. 676:191–196

Kanthal. 2012. *Resistant heating alloys for electric home appliances*. Available: http://www.kanthal.com/globalassets/kanthal-global/downloads/materials-in-wire-and-strip-form/resistance-heating-wire-and-strip/s-ka026-b-eng-2012-01.pdf [July 2016]

Kanthal. n.d. *Fibrothal Heating Modules*. Available:

http://www.kanthal.com/en/products/furnaceproducts-and-heating-systems/heating-modules/fibrothal-heating-modules [July 2016].

Kanthal. n.d. *Resistant heating alloys and systems for industrial furnaces*. Available: http://www.skyscrubber.com/CTL%20-%20Hydrogen%20Generator%20-%20Kanthal%20%20Resistance%20heating%20alloys%20and%20systems%20for%20industrial%20furnaces.pdf [July 2016]

Karadeniz, E., Gurcan, C., Ozgen, S. & Aydin, S. 2007. Properties of alumina based low-cement self flowing castable refractories. *European Ceramic Society*. 27:1849–1853.

Kutz, M. Ed. 2013. *Handbook of measurement in science and engineering*. New Jersey: John Wiley and Sons.
Available:
http://library.books24x7.com.libproxy.cput.ac.za/assetviewer.aspx?bookid=51157&chunkid=1&rowid=2 [Accessed February 8, 2017]

Loveday, M.S., Gray, T. & Aegerter, J. 2004. *Tensile Testing of Metallic Materials: A Review*, Available: http://www.npl.co.uk/upload/pdf/test_method_review.pdf [Accessed March 7, 2016].

Lynch, K. 201. Impirical PID gain tuning [Video file]. Available: https://www.youtube.com/watch?v=uXnDwojRb1g&t=264s [December, 2015]

Lynon, D.A., Keeney, R.M. & Cullen, J.F. 1914. *The electric furnace in metallurgical work*. Washington, D.C.

Mills-Brown, J., Potter, K., Foster, S. & Batho, T., 2013. The development of a high temperature tensile testing rig for composite laminates. *Composites: Part A*. 52:99–105.

Motzfeldt, K., 2013. *High temperature experiments in chemistry and materials science.* 1st ed. Chichester: John Wiley & Sons. Available: CPUT Libraries Catalogue [2016, April].

Msomi, V. & Oliver, G.J. 2016. Smart morphing based on shape memory alloy plate. *Journal of Engineering, Design and Technology*. 14(3):475–488.

Mullinger, P. & Jenkins, B. 2013. *Industrial and Process Furnaces : Principles, Design and Operation.* 2nd ed. Waltham: Butterworth-Heinemann. Available: CPUT Libraries Catalogue [2016, April]

Refractory Lining. 2010. *Insulating Refractories*. Available: http://viewforyou.blogspot.co.za/2010/03/insulating-refractories-part-i.html. [August 2016]

Sachithanandam, Z. 2015. *Electrical heating - part - 02 - design of heating element and properties of a heating element.* [Video file]. Available: https://www.youtube.com/watch?v=aMwP2XwCxv4&t=335s [June 2016].

Samuelsson, P. 2017. Management of technology in the process industries: Matching markets and machines. Master of Applied Science Thesis. Royal Institution of Technology.

Scheunis, L., Fallah-Mehrjardi, A., Campforts, M., Jones, P. T., Blanpain, B., Malfliet, A. & Jak, E. 2015. Effect of a temperature gradient on the phase formation inside a manesia-chromite refractory in contact with a non-ferrous PbO-SiO_2-MgO slag. *Journal of the European Ceramic Society*. 35(10):2933–2942.

Shaw, J.A. & Kyriakides, S. 1995. Thermomechanical aspects of NiTi. *Journal of the Mechanics and Physics of Solids*. 43(8):1243–1281.

Shimizu, T., Matsuura, K., Furue, H. & Matsuzak, K. 2013. Thermal conductivity of high porosity alumina refractory bricks made by a slurry gelation and foaming method. *Journal of the European Ceramic Society*. 33(15-16):3429–3435.

Shivasiddaramaiah, A.G., Mallik, U.S., Shivaramu, L. & Prashantha, S. 2016. Evaluation of shape memory effect and damping characteristics of Cu-Al-Be-Mn shape memory alloys. *Perspectives in Science*. 8:244–246.

Shlyannikov, V.N., Tumanov, A. V. & Zakharov, A.P. 2014. The mixed mode crack growth rate in cruciform specimens subject to biaxial loading. *Theoretical and Applied Fracture Mechanics*. 73:68–81.

Simonson, J.R. 1975. *Engineering Heat Transfer*, London: The MacMillan Press.

Srinivasan, A. V. & McFarland, D.M. 2001. *Smart Structures*, New York: The Press Syndicate of The University of Cambridge.

Temel, S., Yagli, S. & Goren, S. 2013. *Discrete time control systems*. (Recitation 4 report). Middle East Technical University. Available: https://www.scribd.com/document/209613239/EE402Recitation

Venturini, E., Vassura, I., Zanetti, C., Pizzi, A., Toscano, G. & Passarini, F. 2015. Evaluation of non-steady state condition contribution to the total emissions of residential wood pellet stove. *Energy*. 88:650–657.

Vert, T. 2016. Refractory Material Selection for Steelmaking. *American Ceramic Society Bulletin*. 95(2):23–29.

Warwick, K. 1996. *An introduction to control systems*. Singerpore: World Scientific Publishing.

Yarlagadda, B. 2002. Elevated temperature mechanical properties and corrosion characteristics evaluation of alloy HT-9. MSc Thesis. University of Nevada.

Zivcová, Z., Gregorova, E., Pabst, W., Smith, D. S., Michot, A. & Poulier. 2009. Thermal conductivity of porous alumina ceramics prepared using starch as a pore-forming agent. *Journal of the European Ceramic Society*. 29(3):347–353.

Zuda, L. & Cerny, R. 2009. Measurement of linear thermal expansion coefficient of alkali-activated aluminosilicate composites up to 1000^{o}C. *Cement & Concrete Copsites*. 31:263–267.

APPENDICES

APPENDIX A

DETAILED DRAWINGS OF THE CHAMBER

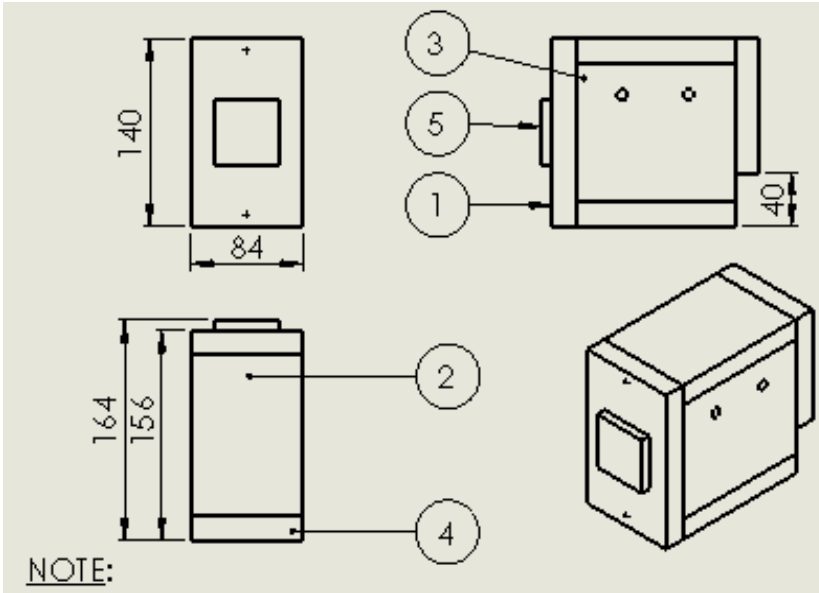

NOTE:

1. Use wood glue to join parts 3 and 4
2. Insert the PID into part 1before joining it onto the previously glued parts
3. Connect electriccables from the PID and then screw part 1 onto the glued parts

ITEM NO.	PART NUMBER	DESCRIPTION	QTY.
1	box-front		1
2	box-topbottom		2
3	box-side		2
4	box-back		1
5	PID		1
6	SSR		1

Figure A1: Control box

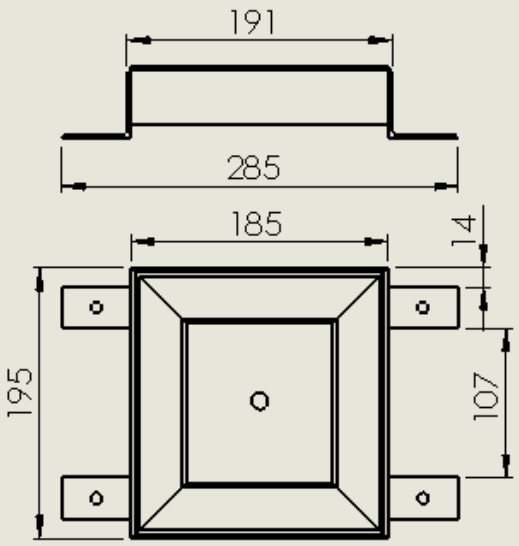

NOTE:

1. Weldments at the miter joint done at the top then drinded off.
2. The sheet metal arc welded onto the mitered frame.

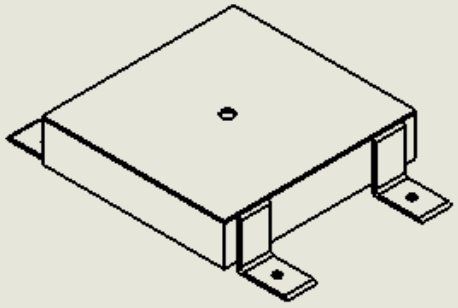

ITEM NO.	PART NUMBER	DESCRIPTION	QTY.
1	Frame part 1	40 x 40 x 3 x 191 Angle iron	2
2	Frame part 2	40 x 40 x 3 x 195 Angle iron	2
3	Top bracket	50 x 50 x 3 x 30 Angle iron	4
4	Top plate	185 x 195 x 3 sheet metal	1

Figure A2: Top shell

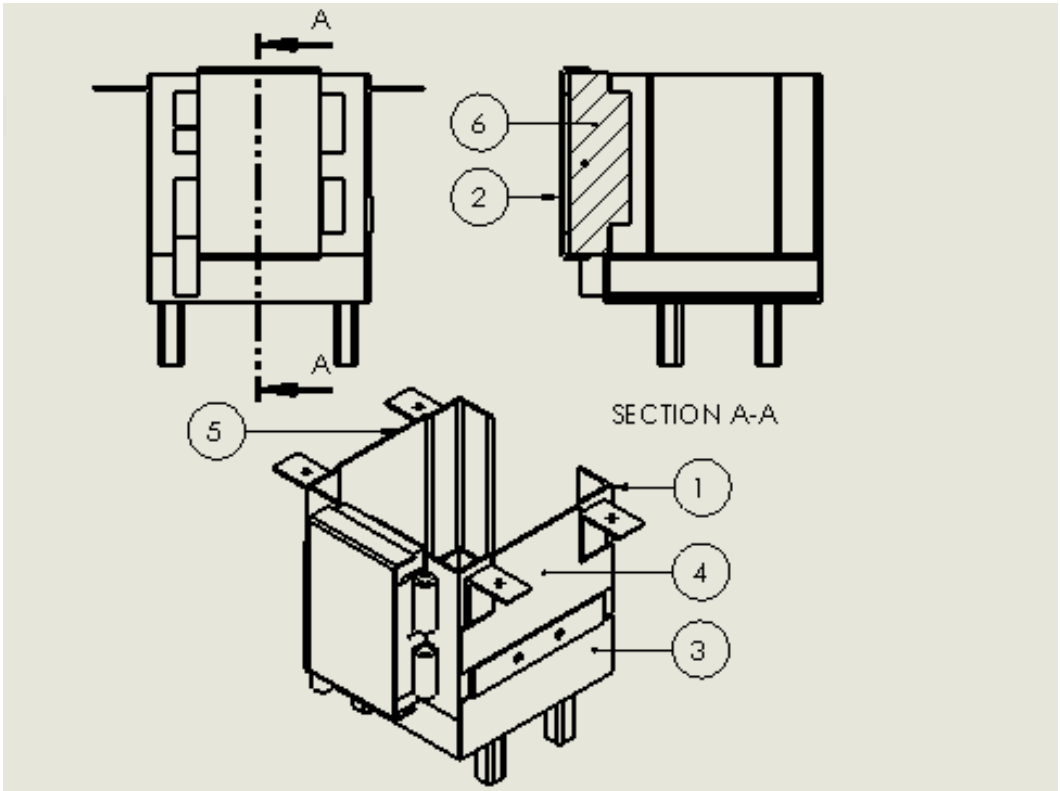

ITEM NO.	PART NUMBER	DESCRIPTION	QTY.
1	Main frame		1
2	Door cover		1
3	Bottom side plate		1
4	Top side plate		1
5	Frame side plate RH		1
6	Door inner		1

Figure A3: Bottom shell

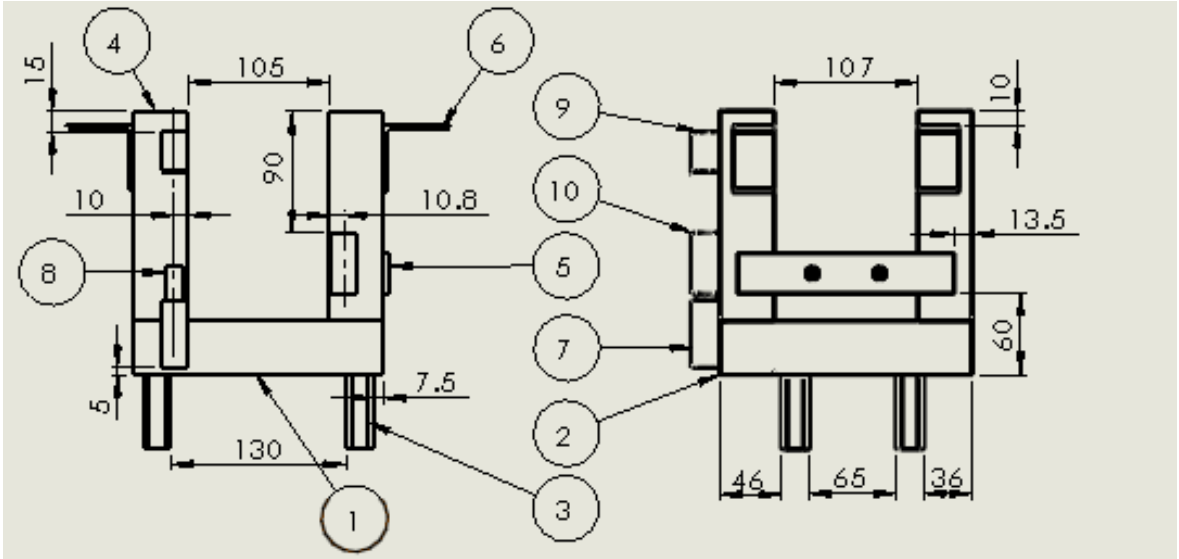

ITEM NO.	QTY.	DESCRIPTION	LENGTH
1	2	L 40 X 40 X 3	185
2	2	L 40 X 40 X 3	187
3	4	TUBE, SQUARE 20 X 20 X 2	55
4	4	L 40 X 40 X 3	155
5	1	FLAT, BAR 35 x 5	160
6	4	L 50 X 50 X 3	30
7	1	ROUND BAR, dia 20	50
8	1	ROUND BAR, dia 12	25
9	1	ROUND BAR, dia 20	30
10	1	PIPE, dia 20 x 4	45

Figure A4: Bottom frame

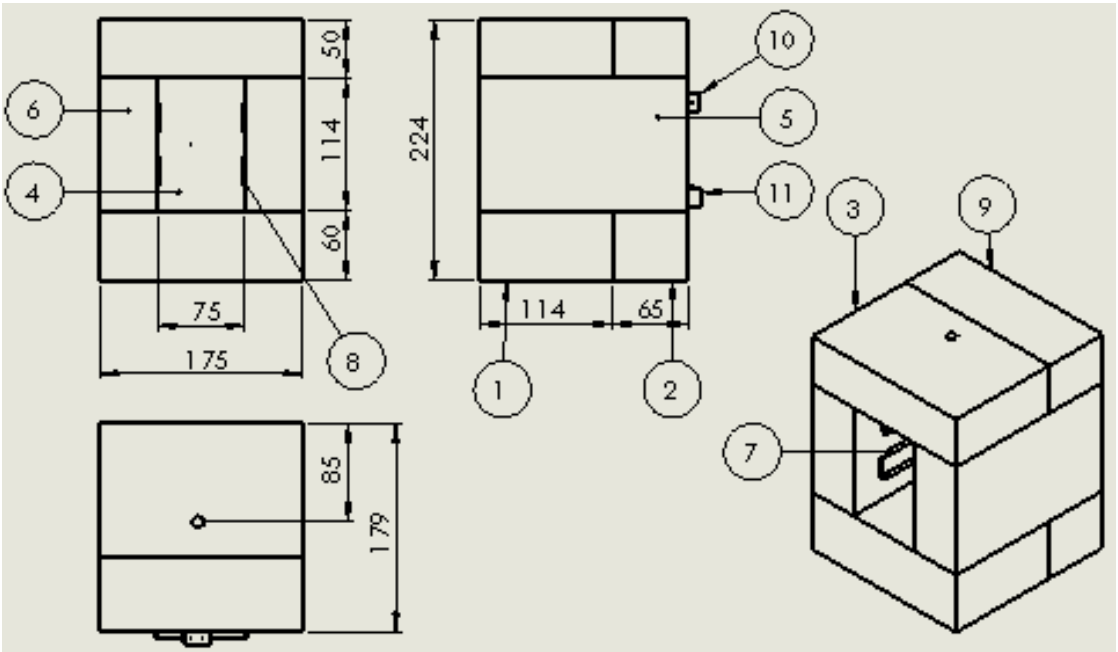

ITEM NO.	PART NUMBER	DESCRIPTION	QTY.
1	Back front brick		1
2	Bottom brick		1
3	Top front brick		1
4	Back brick		1
5	Side brick 1		1
6	Side brick 2		1
7	Heating element 1		1
8	Heating element 2		1
9	Top back brick		1
10	Connector 1		1
11	Connector 2		1

Figure A5: Refractory lining

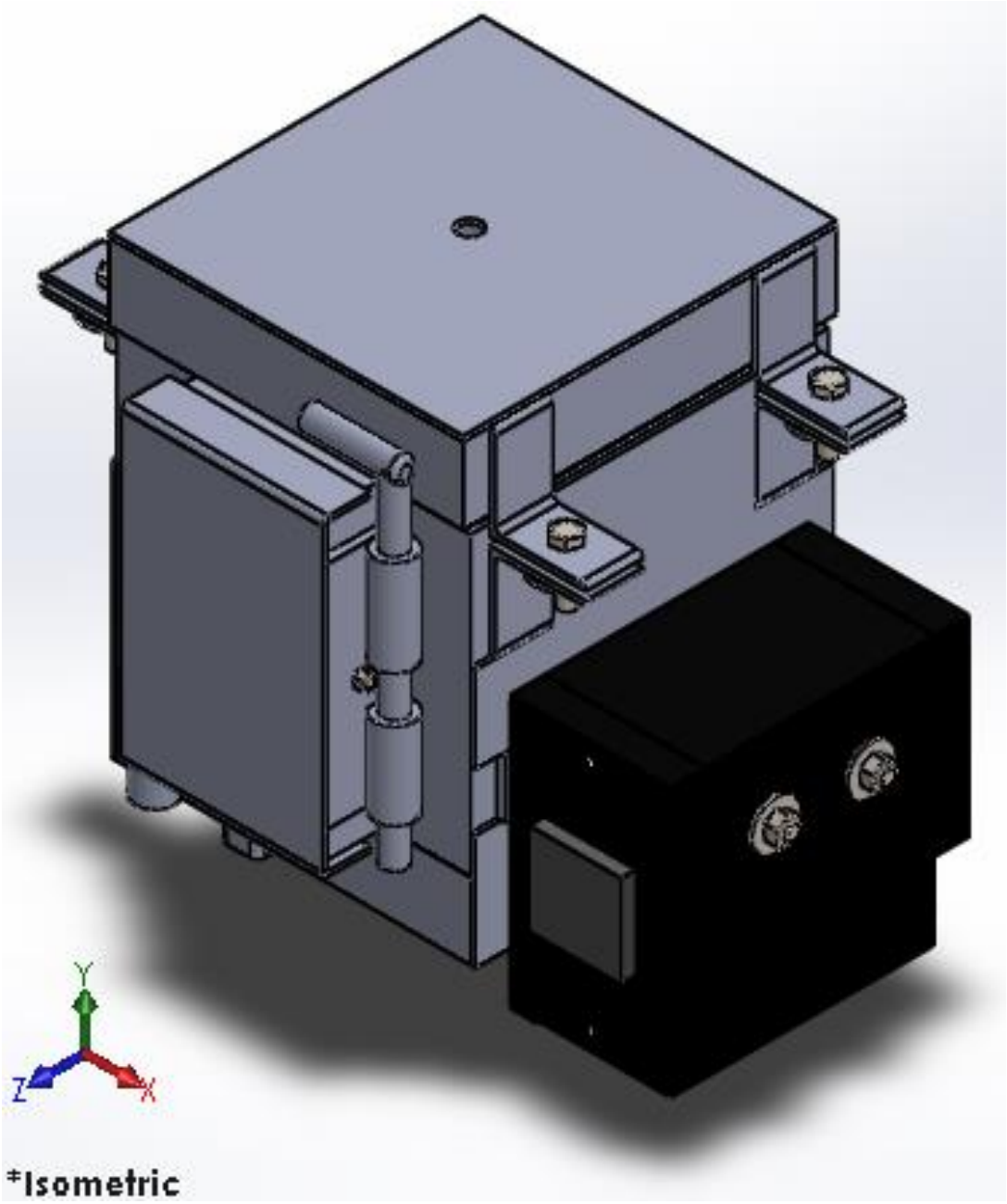

Figure A6: Isometric drawing of thermal chamber

APPENDIX B

TEMPERATURE- TIME PROFILES

Table B1: P-system parameters

Set	Parameter		
	P	I	D
P20	20	0	0
P30	30	0	0
P80	80	0	0

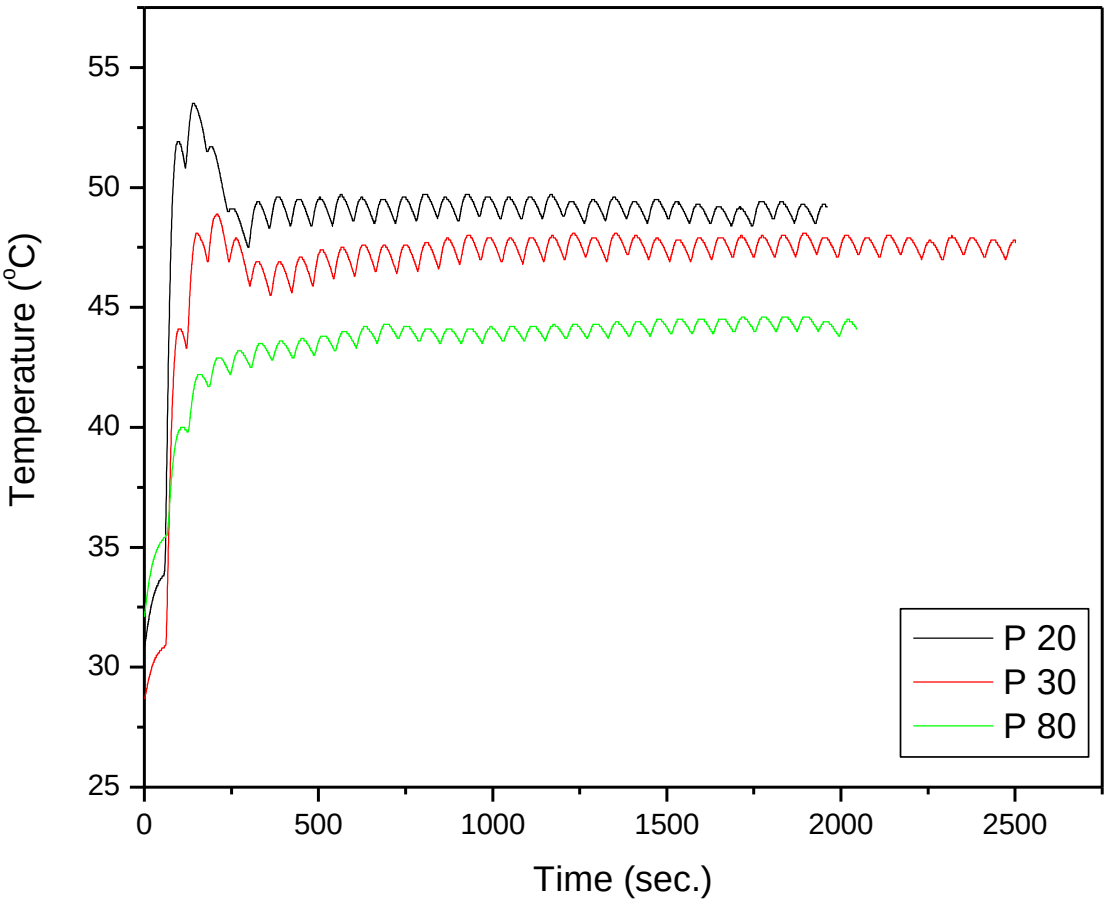

Figure B1: Temperature – time graph for P-system at 50°C set point

Table B2: P-system parameters

Set	Parameter		
	P	I	D
P160	160	0	0
P190	190	0	0
P210	210	0	0

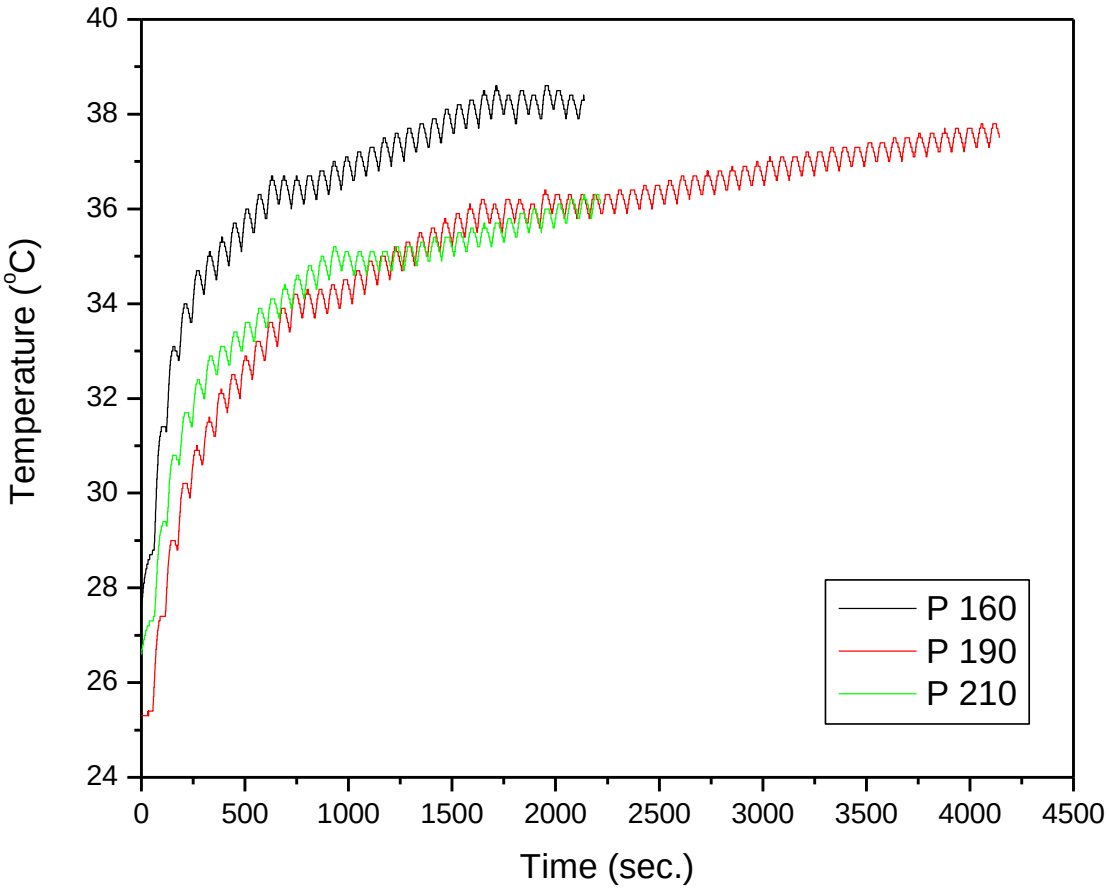

Figure B2: Temperature – time graph for P-system at 50°C set point

Table B2: P-system parameters

Set	Parameter		
	P	I	D
P1	1	0	0
P_{max}	999.9	0	0

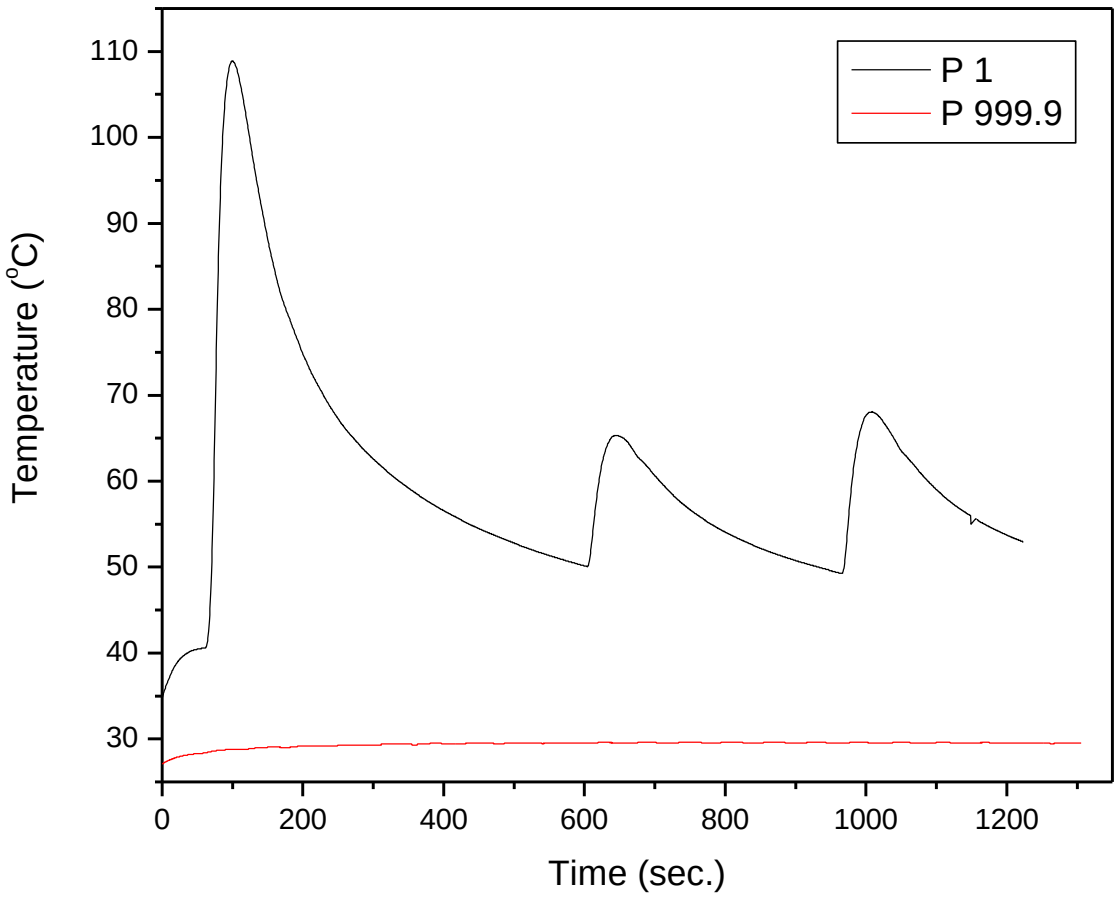

Figure B4: Temperature – time graph for P-system of maximum and minimum at 50°C set point

Table B3: PI-system parameters

Set	Parameter		
	P	I	D
PI 10	1	10	0
PI 11	1	100	0
PI 12	1	1000	0

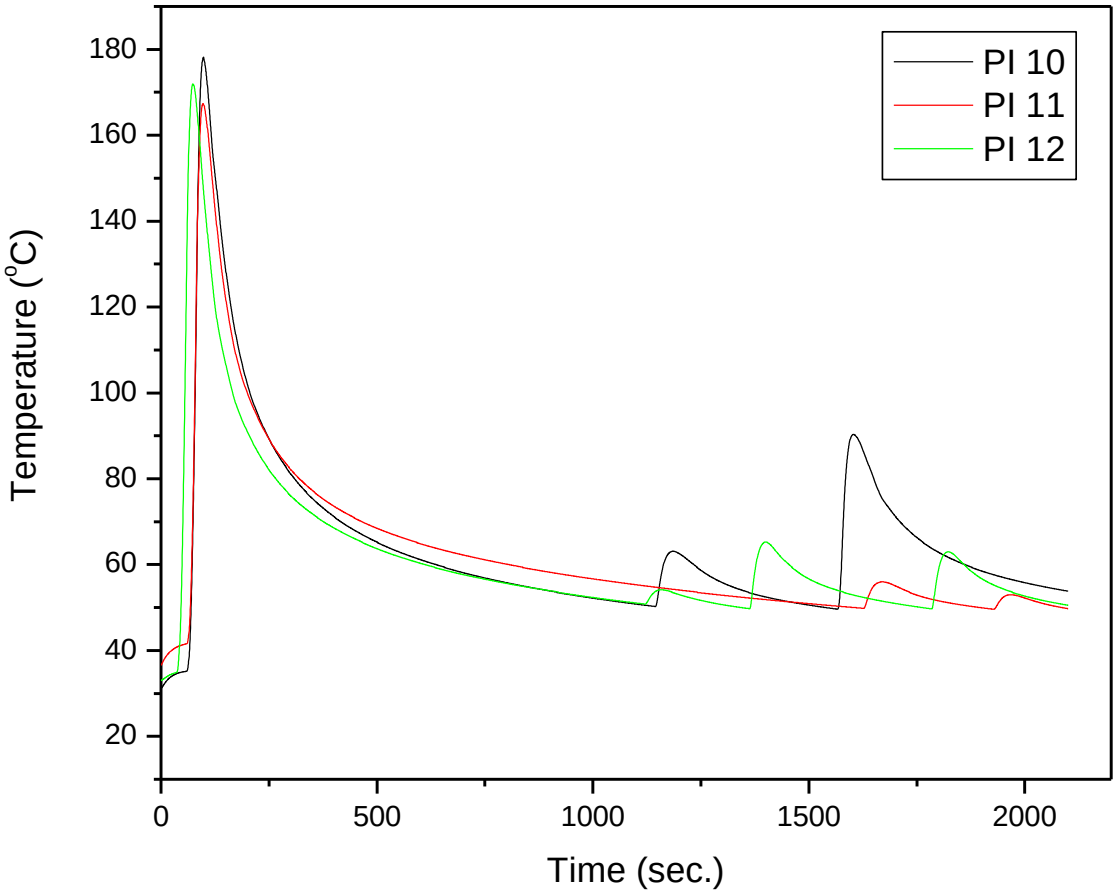

Figure B5: Temperature – time graph for PI-system at 50°C set point

Table B4: PD-system parameter

Set	Parameter		
	P	I	D
PI 10	1	0	10
PI 11	1	0	425
PI 12	1	0	950

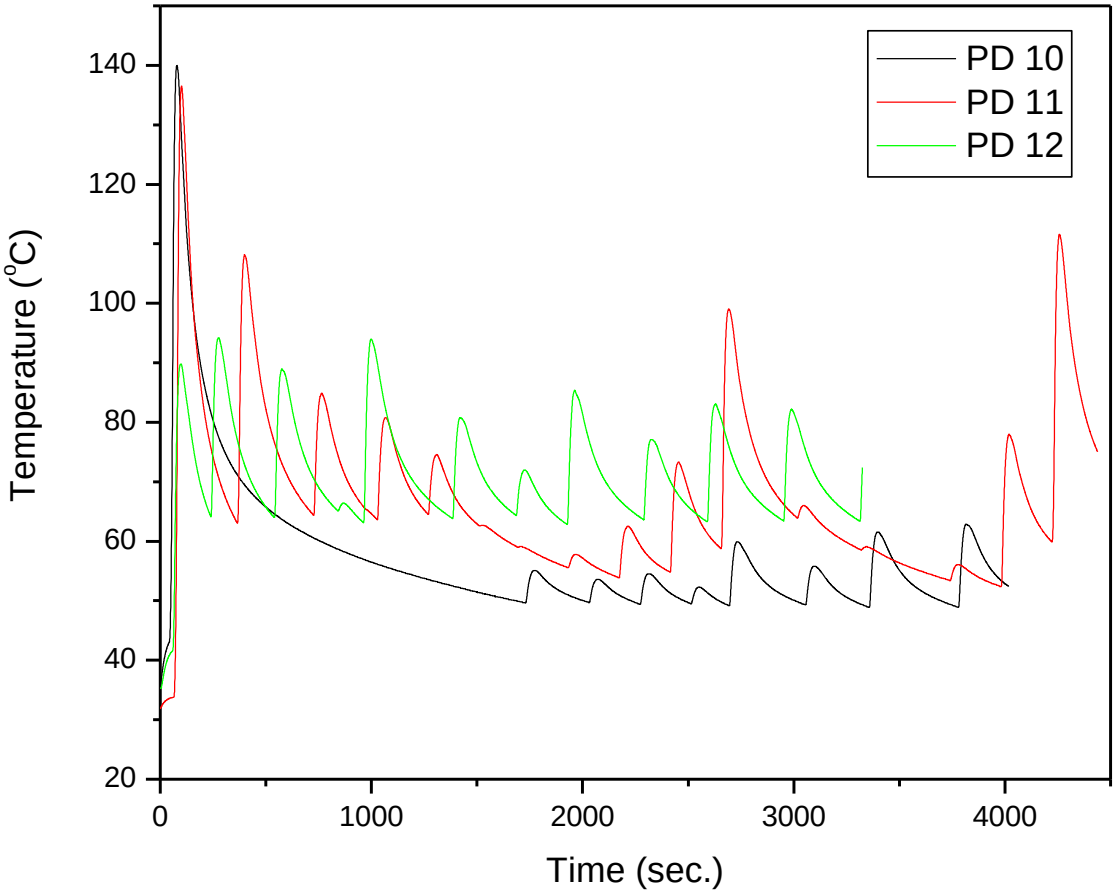

Figure B6: Temperature – time graph for PD-system 4 at 50°C set point

APPENDIX C

CONTROLLED TENSILE TEST RESULTS

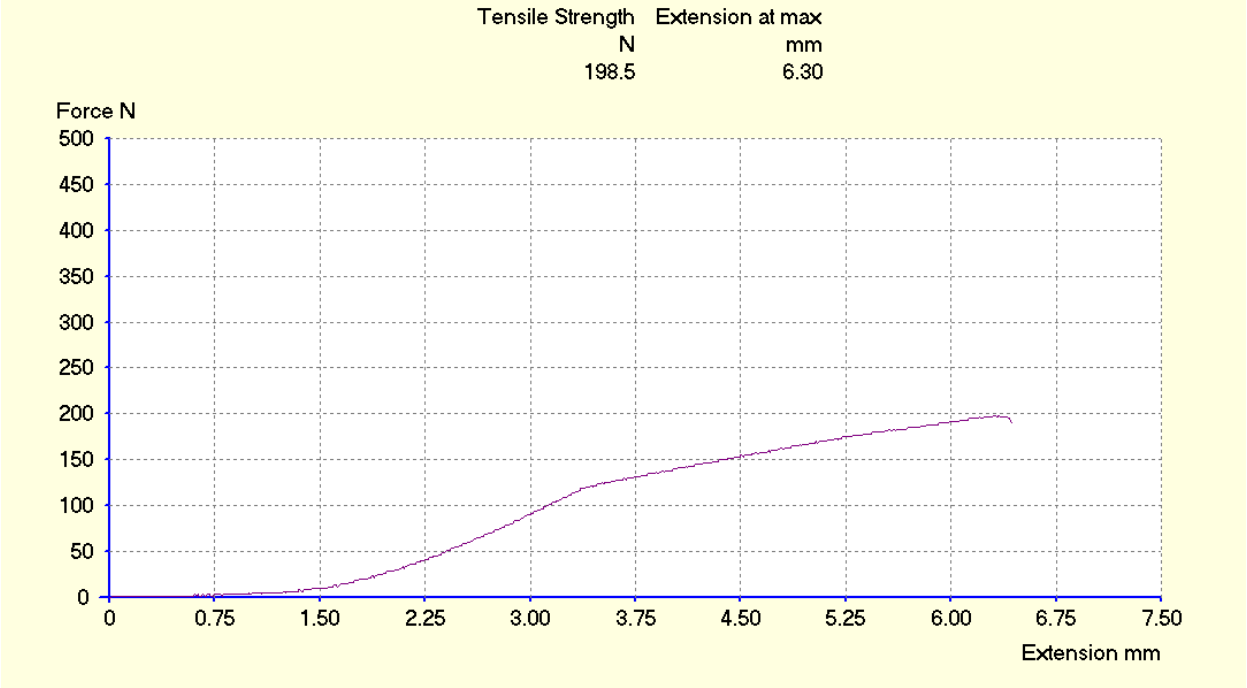

Figure C1: SMA tensile test at room temperature of SMA wire

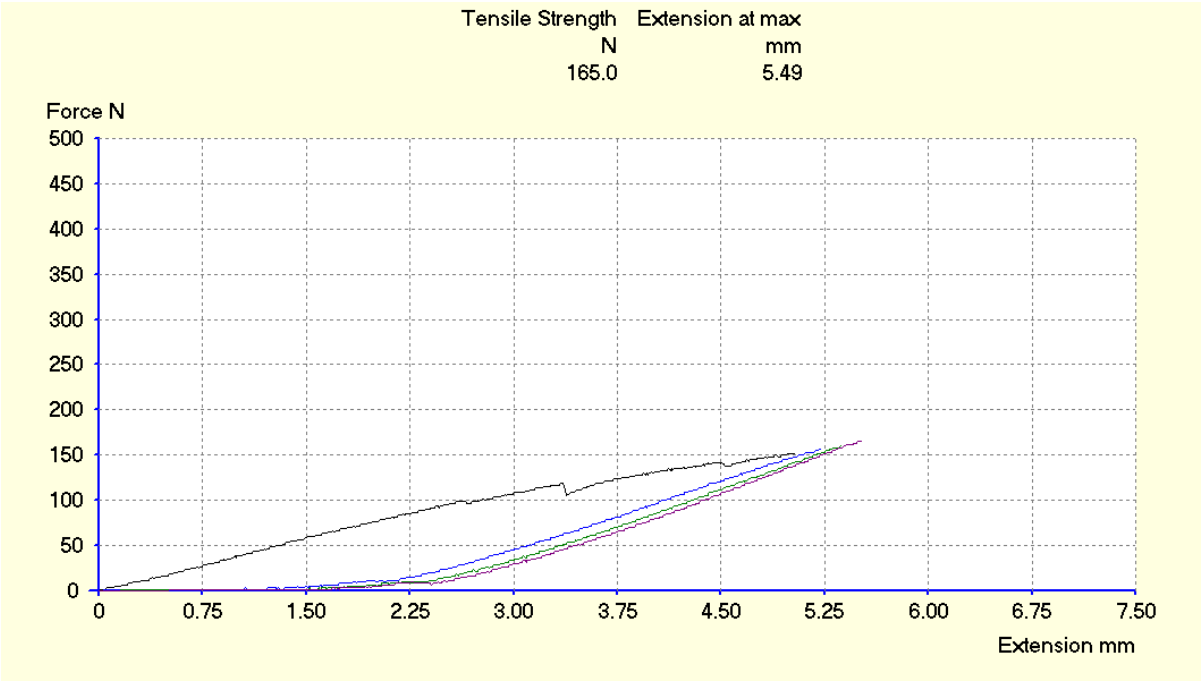

Figure C2: Controlled tensile test at 25°C of SMA wire

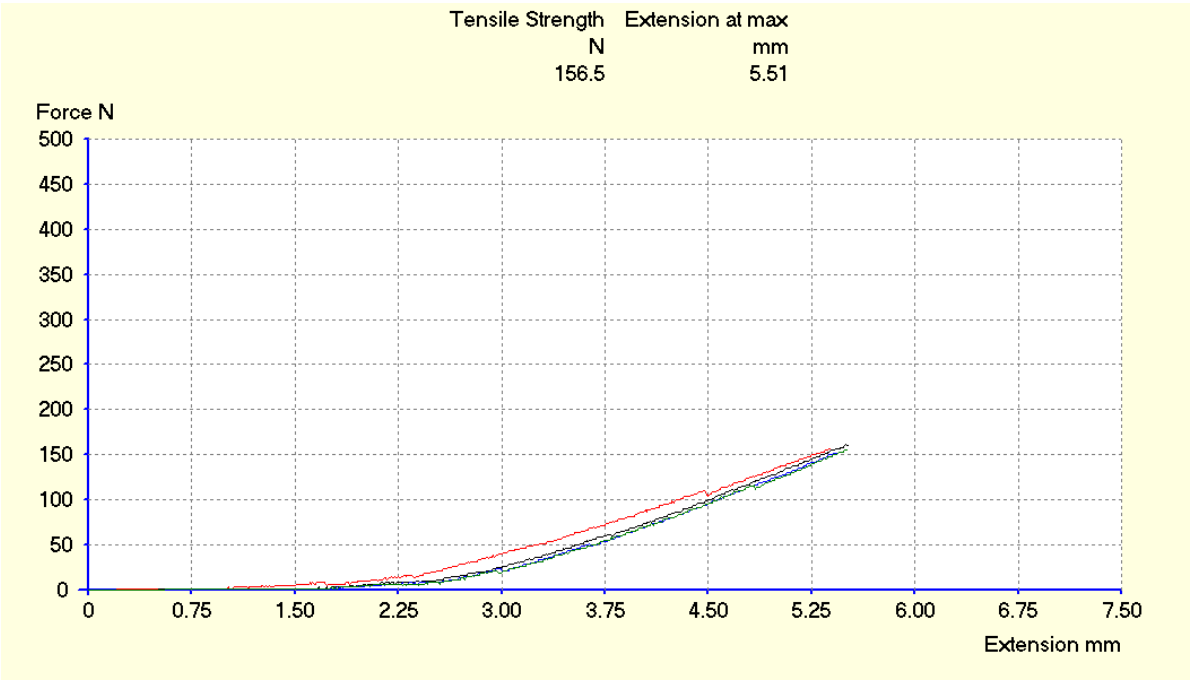

Figure C3: Controlled tensile test at 40°C of SMA wire

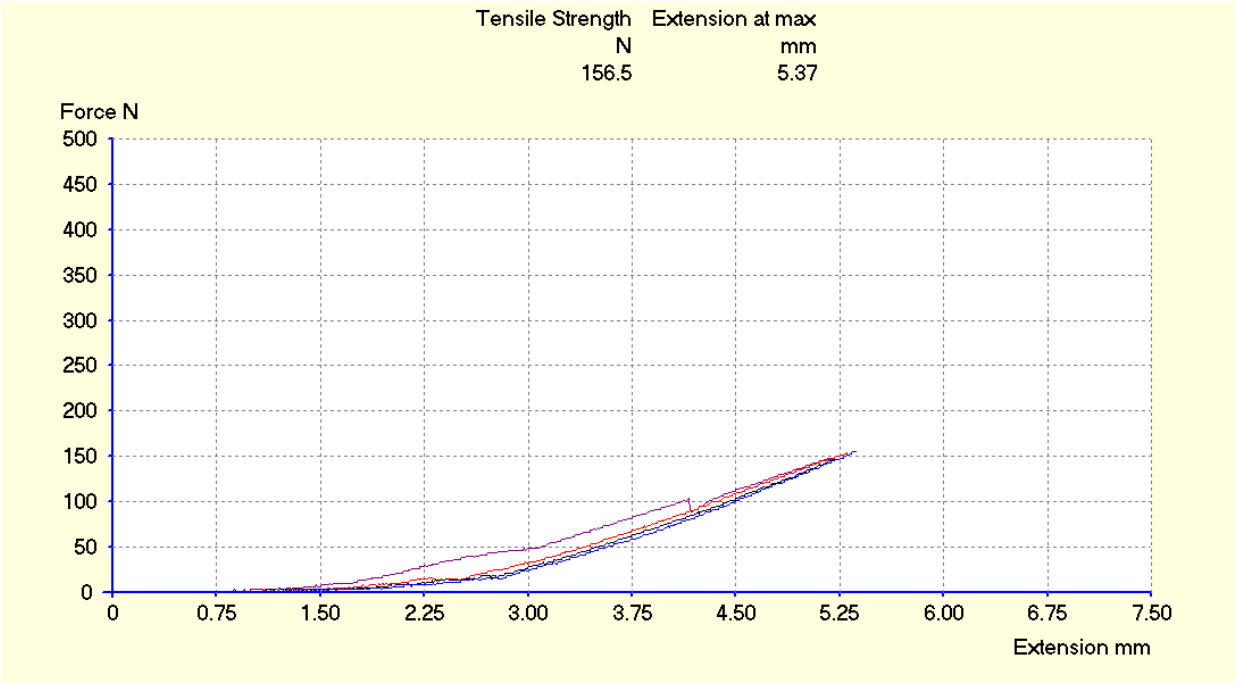

Figure C4: Controlled tensile test at 60°C of SMA wire

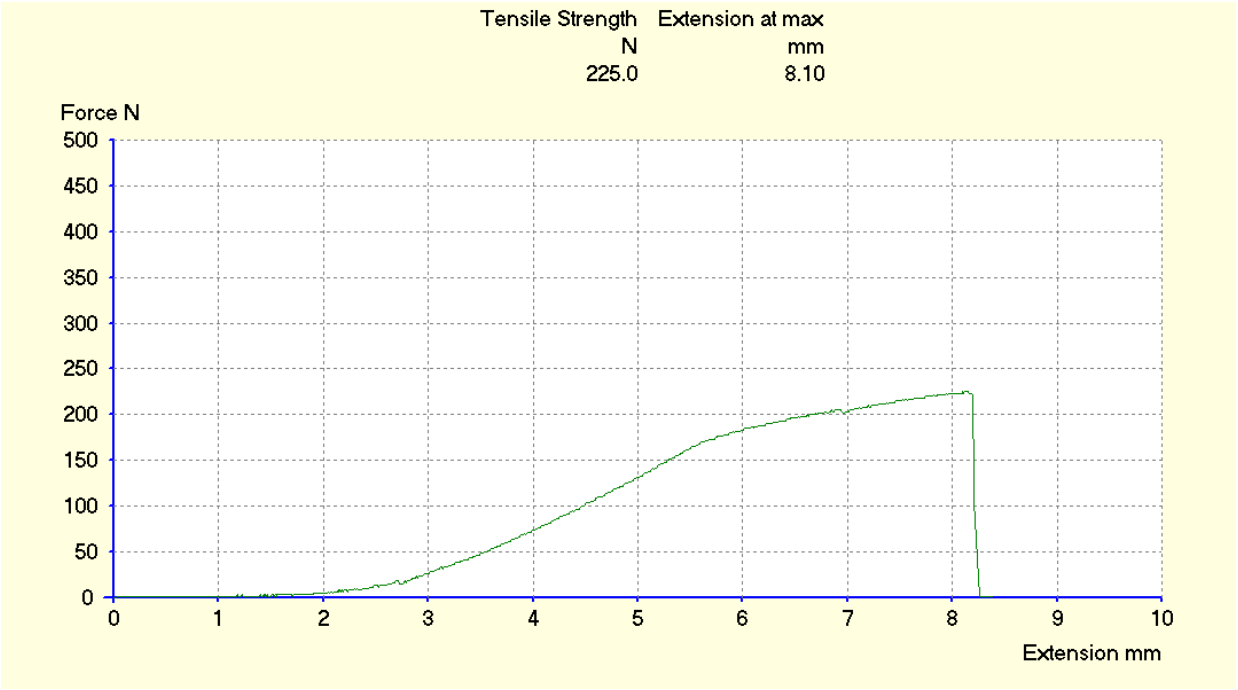

Figure C5: Controlled tensile test at 70°C of SMA wire